CIVIL ENGINEERING STUDIES
STRUCTURAL RESEARCH SERIES NO. 304

THE ANALYSIS OF SHALLOW SHELL STRUCTURES BY A DISCRETE ELEMENT SYSTEM

by
B. MOHRAZ
and
W. C. SCHNOBRICH

A Report on a Research
Program Carried Out
under
National Science Foundation
Grant No. GK-538

UNIVERSITY OF ILLINOIS
URBANA, ILLINOIS
MARCH, 1966

THE ANALYSIS OF SHALLOW SHELL STRUCTURES BY A DISCRETE ELEMENT SYSTEM

by

B. MOHRAZ

and

W. C. SCHNOBRICH

A Report on a Research
Program Carried Out
under
National Science Foundation
Grant No. GK-538

UNIVERSITY OF ILLINOIS
URBANA, ILLINOIS
MARCH, 1966

ACKNOWLEDGMENTS

The results reported herein were obtained in the course of a research study conducted in the Department of Civil Engineering, University of Illinois. This report is based on a thesis by Bijan Mohraz under the direction of Professor Arthur R. Robinson, which was submitted in partial fulfillment of the requirement for the degree of Doctor of Philosophy in Civil Engineering in the Graduate College of the University of Illinois.

The investigation was made possible by the National Science Foundation, under Grant NSF GK-538.

The authors express their appreciation to Dr. John W. Melin for his valuable suggestions regarding the development of the computer program.

TABLE OF CONTENTS

TABLE OF CONTENTS (Continued)

LIST OF TABLES

LIST OF FIGURES

LIST OF FIGURES (Continued)

INTRODUCTION

1.1 General

Shell structures, both from the point of view of structural efficiency and esthetic value, are frequently used to cover large, column-free spaces. Determinations of the magnitude of stresses and their distribution into the shell is of necessity in the design of these structures.

In the interior regions of a shell, away from the supports, the loads are carried mainly by in-plane forces. The membrane theory provides a good estimate of stresses for design purposes. However, in the regions close to the supports, bending stresses are developed as the results of the sharp change in the stiffnesses from that of the shell to that of the edge member.

For shells with simple geometry, such as cylindrical and spherical shells, bending solutions are available for a variety of loadings and support conditions. However, for shells with complex geometry, such as translational shells, bending solutions exist only for a limited number of cases with simple loadings and support conditions. The support conditions for which solutions have been found are rarely those in practical applications. Usually the governing equations are reduced to two equations in terms of a stress function and the radial displacement [13]*. A Levy type solution can be obtained when at least two edges are simply supported. But these supports are usually a poor idealization of actual supports.

One shell surface of particular interest is the hyperbolic paraboloid bounded by the characteristic lines of the surface. A variety of shapes can be

---

* Numbers in brackets refer to references in the Bibliography.

formed by different combinations of hyperbolic paraboloid units. Due to construction economy and the inherent beauty of these shapes, they have been widely used in recent years. The difficulties encountered in the analysis of these shells and their extensive use have led to numerous studies of their structural behavior. The edge disturbance from a straight boundary penetrates into the shell further than the edge disturbance from a curved boundary [4]. Therefore, a bending analysis which takes into account the effect of supporting the shell by an edge member is very important in the design of long span hyperbolic paraboloids. Because of the asymmetric relation between the stress function and the radial displacement in the governing equations of hyperbolic paraboloid, a Levy type solution such as the one used for cylindrical shells leads to unrealistic boundary conditions [5]. This is due to the absence of suitable orthogonal functions.

Approximate methods have been used whenever the exact methods have failed to yield the desired solution. Variational procedures, such as the methods of Ritz, Galerkin, Kantorovich, etc., are available for the solution of boundary value problems. A combination of Kantorovich's and Galerkin's methods has been used to obtain a solution for a hyperbolic paraboloid with simply supported and clamped boundaries [5]. For shells of arbitrary shape, the selection of approximate functions is usually difficult and the integration of these functions is very involved.

Numerical procedures, such as finite differences, have been used to solve the complex differential equations encountered in shell structures [9,10,17]. The use of the method of finite differences in shells frequently results in a set of inconsistent difference equations. This inconsistency can be avoided if the tangential displacements are properly specified [6,14,16].

A still different approach to the problem is the use of models to simulate the shell structure. Hrennikoff [12] replaced the continuous structure by a system of elastic bars. Yettram and Husain [19] used the system of elastic bars to obtain solutions to plate problems. Parikh [15] and Benard [2] applied this method for cylindrical shells. A different model which replaces the continuum by a system of finite plate elements has been used by Clough [7,8]. Zienkiewicz and Gheung [20,21] have applied the method to orthotropic slabs and arch dams. Discrete models consisting of rigid bars and deformable nodes have been used by Ang and Newmark [1] to obtain solutions in plates. Schnobrich [16] used a discrete model for cylindrical shells. One of the advantages of the discrete model is that a consistent set of equations is obtained.

1.2. Objective of Study

With rapid advancements in computer technology, one can now obtain solutions of complex shell problems which previously were not possible because of computational work involved. The objective of this study is to develop a discrete model to simulate a variety of shell structures. The classical shell theory will be used as a guide in the development of the model. The generality of the model is illustrated by presenting numerical examples and comparing them with existing solutions whenever possible.

1.3. Nomenclature

The symbols used in this study are defined when they first appear. For convenience they are summarized below:

a = shell span in x direction

b = shell span in y direction

c = rise or sag of hyperbolic paraboloid bounded by the characteristic lines of the surface

d = twist of element i-1j-1, i+1j-1, i+1j+1, i-1j+1

E = modulus of elasticity

h = shell thickness

L_x = grid length in x direction

L_y = grid length in y direction

M_{xij} = moment about y-axis in deformable node ij

M_{yij} = moment about x-axis in deformable node ij

M_{xyij} = twisting moment in deformable node ij

N_{xij} = membrane force in x direction in deformable node ij

N_{yij} = membrane force in y direction in deformable node ij

N_{xyij} = in-plane shear force in deformable node ij

q = external load

Q_x = vertical shear force at a section perpendicular to x-axis

R_x = radius of curvature in x direction

R_y = radius of curvature in y direction

t = distance between the extensional elements

u_{i+1j} = displacement of point i+1j in x direction

v_{ij+1} = displacement of point ij+1 in y direction

w_{ij} = displacement of deformable node ij in z direction

$\overline{X}$ = external load in x direction

$\overline{Y}$ = external load in y direction

$\overline{Z}$ = external load in z direction

α = angle between rigid bars in xz plane

β = angle between rigid bars in yz plane

ϵ_{xij} = extensional strain in x direction at deformable node ij

ϵ^{u}_{xij} = extensional strain due to u displacement in x direction at deformable node ij

ϵ^{w}_{xij} = extensional strain due to w displacement in x direction at deformable node ij

ϵ_{yij} = extensional strain in y direction at deformable node ij

ϵ_{xyij} = shear strain at deformable node ij

$\epsilon^{u,v}_{xyij}$ = shear strain due to u and v displacements at deformable node ij

ϵ^{w}_{xyij} = shear strain due to w displacement at deformable node ij

θ_{xi+1j} = rotation of bar ij, i+2j in x direction

θ_{yij+1} = rotation of bar ij, ij+2 in y direction

ν = Poisson's ratio

σ_{xij} = extensional stress in x direction at deformable node ij

σ^{b}_{xij} = flexural stress in x direction at deformable node ij

τ_{xy} = shear stress

φ_{x} = opening angle in x direction

φ_{y} = opening angle in y direction

χ_{xij} = flexural strain in x direction at deformable node ij

χ_{yij} = flexural strain in y direction at deformable node ij

χ_{xyij} = twisting strain at deformable node ij

METHOD OF ANALYSIS

2.1. General

Although specialized methods of analysis, such as Levy solution, Ritz and Galerkin methods, etc., have certain advantages for a particular problem, it is desirable to have a general method of analysis which can be used for a variety of shell surfaces. Different boundary conditions, different values of Poisson's ratio, and different combinations of loading should not present any difficulty in the method of analysis. The method should be adaptable to non-linear problems, orthotropic shells, and shells with variable thickness.

One such method is the use of a discrete model consisting of rigid bars and deformable nodes similar to that proposed by Schnobrich [16]. Since the material properties of the shell are concentrated at the deformable nodes, the method can be used to study the behavior of shells with different material properties in the two directions. It can also be used to analyze shells with variable thickness. The forces and the moments are constant across each node, thus, non-linear material properties would not present any difficulty in the use of the model.

Because of the complexity of the equations governing the behavior of the model, it is advantageous to generate and solve the resulting set of equations within a digital computer. Due to the effort involved in the development of individual computer programs for various cases, it is preferable to develop a single general computer program which can be used and can easily be extended to a variety of shell problems. Although such a computer program can become very complex, once it is completed many shell surfaces with various

loadings and support conditions can economically be investigated without much additional programming.

The equations governing the behavior of the model are formulated for a general doubly curved surface using orthogonal coordinates. However, the coordinate lines are not necessarily the set which coincides with the lines of principal curvature.

2.2. Description of the Model

The discrete model employed in this study consists of rigid bars and deformable nodes arranged as shown in Figs. (1,2). The nodes have extensional and shear properties similar to those of the real material. At the midpoint of each rigid bar there is a groove with a circular hole at its center, Fig. 3. The rigid bars are connected to each other at these grooves by a pin which is inserted in the holes. With this type of connection, the two bars move independently of each other in the radial direction. However, the rotation of one bar would cause a twist in the other bar.

This model is a modification of the one used previously for cylindrical shells [16]. By specifying the tangential displacements at the same point, the extensional and shear behaviors are no longer separated from each other. The model can thus be used to study the nonlinear material behavior of shells based on accepted yield theories. It also makes it possible to formulate the governing equilibrium equations of hyperbolic paraboloid shells bounded by characteristics as well as other shells of negative curvature.

When the model is used for the analysis of shell structures, the deformable nodes are placed at the intersections of the surface generators, Fig. 1. For shallow shells the generators are usually approximated by circular

vary at each point. It is therefore convenient to adopt a moving triad of axes. When the origin of the coordinate system is placed at the deformable node ij, the x and y axes are set along the bisectors of the angles formed by the rigid bars in the xz and the yz planes respectively. The z axis is directed along the perpendicular to the plane containing the bisectors (i.e., the tangential plane). The positive direction of z axis is into the plane of the paper, thus, resulting in a left handed coordinate system. By rotating this coordinate system through angles $\beta/2$ and $\alpha/2$ about the x and y axes respectively, the desired coordinate system at points ij-1, i+1j, ij+1, and i-1j is obtained.

Throughout this study, the strains, the forces, and the moments are formulated for deformable node ij. Node ij may be a typical interior node, a node near the boundary, or a node on the boundary. The equilibrium equation in the x direction is formulated for point i+1j which is located one-half space from the node ij, in the positive x direction. Similarly the equilibrium equation in the y direction is formulated for point ij+1 which is located one-half space from the node ij, in the positive y direction. The equilibrium equation in the z direction is formulated at point ij. Points i+1j, ij+1, and ij may be typical interior points, points near the boundary, or points on the boundary.

2.4. Displacements

Displacements are defined in the following manner:

a. The tangential displacement "u" is defined at the intersection of rigid bars and is directed along the axis of the bar in the x direction.

b. The tangential displacement "v" is defined at the intersection of rigid bars and is directed along the axis of the bar in the y direction.

c. The radial displacement "w" is defined at the deformable node and is directed along the perpendicular to the plane containing the bisectors of the angles formed by the rigid bars (tangential plane).

The positive direction of u, v, and w is the positive direction of x, y, and z axes respectively. Figures 1, 2, and 4 show the manner in which the displacements are defined. The above displacements are only the components of the total displacements at the specified points. The total displacement of any point in a given direction is obtained by proper combination of these displacements.

2.5. Strain-Displacement Relations

To find the extensional strain in the x direction at the deformable node ij, the u displacements of the rigid bars adjoining the node must be transformed to the plane containing the node (tangential plane). The extensional strain due to u displacements (see Fig. 6) is

$$\epsilon^{u}_{xij} = \frac{1}{L_x \cos \alpha/2} (u_{i+1j} - u_{i-1j}) \tag{2.2}$$

The extensional strain due to w displacement of the deformable node ij (see Fig. 7) is

$$\epsilon^{w}_{xij} = \frac{-1}{R_x \cos \alpha/2} w_{ij} \tag{2.3}$$

Therefore, the total extensional strain in the x direction at the node ij is

$$\epsilon_{xij} = \frac{1}{L_x \cos \alpha/2} (u_{i+1j} - u_{i-1j}) - \frac{1}{R_x \cos \alpha/2} w_{ij} \tag{2.4}$$

Similarly the extensional strain in the y direction at the deformable node ij can be written as

$$\epsilon_{yij} = \frac{1}{L_y \cos \beta/2} (v_{ij+1} - v_{ij-1}) - \frac{1}{R_y \cos \beta/2} w_{ij} \tag{2.5}$$

The in-plane shear strain due to tangential displacements surrounding the node ij is

$$\epsilon^{u,v}_{xyij} = \frac{1}{L_y} (u_{ij+1} - u_{ij-1}) + \frac{1}{L_x} (v_{i+1j} - v_{i-1j}) \tag{2.6}$$

Because of the twist of the surface there is also a shear strain due to the normal displacement (see Fig. 8).

$$\epsilon^{w}_{xyij} = - 2 \frac{d}{L_x L_y} w_{ij} \tag{2.7}$$

Therefore, the total shear strain at the deformable node ij is

$$\epsilon_{xyij} = \frac{1}{L_y} (u_{ij+1} - u_{ij-1}) + \frac{1}{L_x} (v_{i+1j} - v_{i-1j}) - 2 \frac{d}{L_x L_y} w_{ij} \tag{2.8}$$

It should be noted that these strains are the average strains through the thickness.

The above strains are due to extension and shear. There are also strains due to bending and twist which result from the rotation of the rigid bars. The rotation of the rigid bar ij, i+2j in the x direction can be seen from Fig. 9 as

$$\theta_{xi+1j} = \frac{1}{L_x} \left[\frac{L_x}{R_x \cos \alpha/2} u_{i+1j} + \frac{1}{\cos \alpha/2} (w_{i+2j} - w_{ij}) \right] \tag{2.9}$$

Similarly the rotation of the rigid bar i-2j, ij in the x direction is

$$\theta_{xi-1j} = \frac{1}{L_x} \left[\frac{L_x}{R_x \cos \alpha/2} u_{i-1j} + \frac{1}{\cos \alpha/2} (w_{ij} - w_{i-2j}) \right] \tag{2.10}$$

The flexural strain in the x direction at the top and the bottom elements of the deformable node ij is obtained from Fig. 10 as

$$\chi_{xij} = \frac{1}{L_x} (\theta_{xi+1j} - \theta_{xi-1j}) \frac{t}{2} \tag{2.11}$$

Substitution for θ_{xi+1j} and θ_{xi-1j} yields

$$\chi_{xij} = \frac{t}{2R_x L_x \text{ Cos } \alpha/2} (u_{i+1j} - u_{i-1j}) + \frac{t}{2L_x^2 \text{ Cos } \alpha/2} (w_{i+2j} - 2w_{ij} + w_{i-2j}) \tag{2.12}$$

Similarly the flexural strain in the y direction at the top and the bottom elements of the deformable node ij is

$$\chi_{yij} = \frac{t}{2R_y L_y \text{ Cos } \beta/2} (v_{ij+1} - v_{ij-1}) + \frac{t}{2L_y^2 \text{ Cos } \beta/2} (w_{ij+2} - 2w_{ij} + w_{ij-2}) \tag{2.13}$$

The twisting strain is obtained from the relative rotation of the four rigid bars surrounding the deformable node ij. Hence,

$$\chi_{xyij} = \frac{1}{L_y} (\theta_{xij+1} - \theta_{xij-1}) \frac{t}{2} + \frac{1}{L_x} (\theta_{yi+1j} - \theta_{yi-1j}) \frac{t}{2} \tag{2.14}$$

Expressions for θ's similar to Eq. (2.9) can easily be obtained by proper use of subscripts. Substitution for θ's yields

$$\chi_{xyij} = \frac{t}{2R_x L_y \text{ Cos } \alpha/2} (u_{ij+1} - u_{ij-1}) + \frac{t}{2R_y L_x \text{ Cos } \beta/2} (v_{i+1j} - v_{i-1j})$$
$$+ \frac{t}{2L_x L_y} \left(\frac{1}{\text{Cos } \alpha/2} + \frac{1}{\text{Cos } \beta/2}\right)(w_{i+1j+1} - w_{i-1j+1} - w_{i+1j-1} + w_{i-1j-1}) \tag{2.15}$$

2.6. Forces and Moments

As was mentioned in Section 2.2, it is assumed that the deformable nodes are in a state of plane stress. The in-plane forces and the bending moments are concentrated at the deformable nodes. The in-plane force in the x direction at the deformable node ij is obtained by multiplying the extensional stress σ_{xij} by the area. Thus,

$$N_{xij} = \sigma_{xij} \left(\frac{L_y}{2}\right) h \tag{2.16}$$

From Eq. (2.1)

$$\sigma_{xij} = \frac{E}{1-\nu^2} \left(\epsilon_{xij} + \nu\epsilon_{yij}\right) \tag{2.17}$$

Substituting for σ_{xij} in Eq. (2.16) we obtain

$$N_{xij} = \frac{Eh}{1-\nu^2} \frac{L_y}{2} \left(\epsilon_{xij} + \nu\epsilon_{yij}\right) \tag{2.18}$$

Similarly

$$N_{yij} = \frac{Eh}{1-\nu^2} \frac{L_x}{2} \left(\epsilon_{yij} + \nu\epsilon_{xij}\right) \tag{2.19}$$

The in-plane shear forces are

$$N_{xyij} = \frac{Eh}{2(1+\nu)} \frac{L_y}{2} \epsilon_{xyij} \tag{2.20}$$

$$N_{yxij} = \frac{Eh}{2(1+\nu)} \frac{L_x}{2} \epsilon_{xyij} \tag{2.21}$$

The expressions for ϵ_{xij}, ϵ_{yij}, and ϵ_{xyij} are given by Eqs. (2.4), (2.5), and (2.8), respectively.

The bending moment in the x direction at the deformable node ij is obtained by taking moments about the mid-depth of the deformable node. Therefore,

$$M_{xij} = -2\left[\sigma^{b}_{xij}\left(\frac{L_y}{2}\right)\frac{h}{2}\right]\frac{t}{2} \tag{2.22}$$

where σ^{b}_{xij} is the stress due to bending and is given by

$$\sigma^{b}_{xij} = \frac{E}{1-\nu^2}\left(\chi_{xij} + \nu\chi_{yij}\right) \tag{2.23}$$

Thus,

$$M_{xij} = -\frac{Eh}{1-\nu^2}\frac{L_y}{2}\frac{t}{2}\left(\chi_{xij} + \nu\chi_{yij}\right) \tag{2.24}$$

Similarly

$$M_{yij} = -\frac{Eh}{1-\nu^2}\frac{L_x}{2}\frac{t}{2}\left(\chi_{yij} + \nu\chi_{xij}\right) \tag{2.25}$$

The twisting moments are

$$M_{xyij} = -\frac{Eh}{2(1+\nu)}\frac{L_y}{2}\frac{t}{2}\chi_{xyij} \tag{2.26}$$

$$M_{yxij} = -\frac{Eh}{2(1+\nu)}\frac{L_x}{2}\frac{t}{2}\chi_{xyij} \tag{2.27}$$

The expressions for χ_{xij}, χ_{yij}, and χ_{xyij} are given by Eqs. (2.12), (2.13), and (2.15), respectively.

To obtain the distribution of the forces and the moments, Eqs. (2.18) through (2.21) and (2.24) through (2.27) are divided by $\frac{L_x}{2}$ or $\frac{L_y}{2}$.

2.7. Equilibrium Equations

The principle of virtual displacement is used to formulate the equilibrium equations governing the behavior of the model. By the principle

of virtual displacement, if the system is in equilibrium the total work done by the internal forces plus the total work done by the external forces is equal to zero for any arbitrary virtual displacement. For example, to obtain the equilibrium equation in the radial direction at a specified node, the node is given a virtual displacement while all other displacements remain fixed. The sum of the works done by the internal and the external forces caused by this virtual displacement is then set equal to zero. The results are a set of linear algebraic simultaneous equations in terms of the three displacements. These equations are solved and the obtained displacements are used to compute the forces and the moments.

The equilibrium equation in the x direction is obtained by giving the intersection of the rigid bars a virtual displacement Δu while keeping all other displacements fixed. Referring to Fig. 5, a virtual displacement Δu_{i+1j}, results in a change in extension and flexure of the nodes ij and i+2j and a change in shear and twist of the nodes i+1j+1 and i+1j-1. The internal work is equal to the negative of the change in the strain energy of the four deformable nodes. Hence,

$$W_{int} = - \sum N \, \Delta\epsilon \, L \tag{2.28}$$

where N and $\Delta\epsilon$ are the force and the strain due to extension, shear, bending, and twist. Substitution for N's and $\Delta\epsilon$'s yields

$$\begin{aligned} W^{u}_{int} = - \frac{Eh}{1-\nu^2} \frac{L_x L_y}{2} \Big[& (\epsilon_{xij} + \nu\epsilon_{yij})\Delta\epsilon_{xij} + (\chi_{xij} + \nu\chi_{yij})\Delta\chi_{xij} \\ & + (\epsilon_{xi+2j} + \nu\epsilon_{yi+2j})\Delta\epsilon_{xi+2j} + (\chi_{xi+2j} + \nu\chi_{yi+2j})\Delta\chi_{xi+2j} \\ & + \frac{1-\nu}{2} (\epsilon_{xyi+1j-1}\Delta\epsilon_{xyi+1j-1} + \chi_{xyi+1j-1}\Delta\chi_{xyi+1j-1} \\ & + \epsilon_{xyi+1j+1}\Delta\epsilon_{xyi+1j+1} + \chi_{xyi+1j+1}\Delta\chi_{xyi+1j+1}) \Big] \end{aligned} \tag{2.29}$$

where $\Delta\epsilon$'s and $\Delta\chi$'s are the incremental strains, i.e.,

$$\Delta\epsilon_{xij} = \frac{1}{L_x \cos \alpha/2} \Delta u_{i+1j}$$

$$\Delta\epsilon_{xi+2j} = \frac{1}{L_x \cos \alpha/2} (-\Delta u_{i+1j}) \tag{2.30}$$

. . . . . .

. . . . . etc.

The external work of the component of the load in the x direction at point i+1j is

$$W^u_{ext} = \bar{X}_{i+1j} \Delta u_{i+1j} \tag{2.31}$$

For equilibrium

$$W^u_{ext} + W^u_{int} = 0 \tag{2.32}$$

Substituting the strain-displacement relations into Eq. (2.29) and then substituting the results into Eq. (2.32), the desired equilibrium equation is obtained. Thus, the equilibrium equation in the x direction at point i+1j is

$$\frac{L_x L_y}{2} \Big[\Big(\frac{1}{\cos^2 \alpha/2} + \frac{t^2}{4R_x^2 \cos^2 \alpha/2} \Big) \frac{1}{L_x^2} (u_{i+3j} - 2u_{i+1j} + u_{i-1j})$$

$$+ \frac{1-\nu}{2} \Big(1 + \frac{t^2}{4R_x^2 \cos^2 \alpha/2} \Big) \frac{1}{L_y^2} (u_{i+1j+2} - 2u_{i+1j} + u_{i+1j-2})$$

$$+ \Big(\frac{1-\nu}{2} + \frac{\nu}{\cos \alpha/2 \cos \beta/2} + \frac{1+\nu}{2} \frac{t^2}{4R_x R_y \cos \alpha/2 \cos \beta/2} \Big) \frac{1}{L_x L_y} (v_{i+2j+1} - v_{i+2j-1}$$

$$- v_{ij+1} + v_{ij-1}) - \Big(\frac{1}{R_x \cos^2 \alpha/2} + \frac{\nu}{R_y \cos \alpha/2 \cos \beta/2} \Big) \frac{1}{L_x} (w_{i+2j} - w_{ij})$$

$$- \left(\frac{1-\nu}{L_x L_y}\right) \frac{d}{L_y} \left(w_{i+1j+1} - w_{i+1j-1}\right) + \left(\frac{t^2}{4R_x \cos^2 \alpha/2}\right) \frac{1}{L_x^3} \left(w_{i+4j} - 3w_{i+2j}\right.$$

$$+ 3w_{ij} - w_{i-2j}) + \frac{t^2}{4R_x \cos \alpha/2} \left(\frac{1-\nu}{2} \frac{1}{\cos \alpha/2} + \frac{1+\nu}{2} \frac{1}{\cos \beta/2}\right) \frac{1}{L_x L_y^2} \left(w_{i+2j+2}\right.$$

$$\left. - 2w_{i+2j} + w_{i+2j-2} - w_{ij+2} + 2w_{ij} - w_{ij-2}\right)\Big] + \frac{1-\nu^2}{Eh} \bar{X}_{i+1j} = 0 \tag{2.33}$$

Similarly the equilibrium equation in the y direction is obtained by giving the intersection of rigid bars a virtual displacement Δv and then satisfying the relation

$$W^v_{ext} + W^v_{int} = 0 \tag{2.34}$$

Finally when the deformable node ij is given a virtual displacement Δw the internal work of the surrounding nodes can be written as

$$W^w_{int} = - \frac{Eh}{1-\nu^2} \frac{L_x L_y}{2} \Big[(\epsilon_{xi-2j} + \nu\epsilon_{yi-2j})\Delta\epsilon_{xi-2j} + (\chi_{xi-2j} + \nu\chi_{yi-2j})\Delta\chi_{xi-2j}$$

$$+ (\epsilon_{xij} + \nu\epsilon_{yij})\Delta\epsilon_{xij} + (\chi_{xij} + \nu\chi_{yij})\Delta\chi_{xij}$$

$$+ (\epsilon_{xi+2j} + \nu\epsilon_{yi+2j})\Delta\epsilon_{xi+2j} + (\chi_{xi+2j} + \nu\chi_{yi+2j})\Delta\chi_{xi+2j}$$

$$+ (\epsilon_{yij-2} + \nu\epsilon_{xij-2})\Delta\epsilon_{yij-2} + (\chi_{yij-2} + \nu\chi_{xij-2})\Delta\chi_{yij-2}$$

$$+ (\epsilon_{yij} + \nu\epsilon_{xij})\Delta\epsilon_{yij} + (\chi_{yij} + \nu\chi_{xij})\Delta\chi_{yij}$$

$$+ (\epsilon_{yij+2} + \nu\epsilon_{xij+2})\Delta\epsilon_{yij+2} + (\chi_{yij+2} + \nu\chi_{xij+2})\Delta\chi_{yij+2}$$

$$+ \frac{1-\nu}{2} (\epsilon_{xyi-1j-1} \Delta\epsilon_{xyi-1j-1} + \chi_{xyi-1j-1} \Delta\chi_{xyi-1j-1} + \epsilon_{xyi+1j-1} \Delta\epsilon_{xyi+1j-1}$$

$$+ \chi_{xyi+1j-1} \Delta\chi_{xyi+1j-1} + \epsilon_{xyi+1j+1} \Delta\epsilon_{xyi+1j+1} + \chi_{xyi+1j+1} \Delta\chi_{xyi+1j+1}$$

$$\left. + \epsilon_{xyi-1j+1} \Delta\epsilon_{xyi-1j+1} + \chi_{xyi-1j+1} \Delta\epsilon_{xyi-1j+1} + \epsilon_{xyij} \Delta\epsilon_{xyij})\right] \tag{2.35}$$

The external work is

$$W^{w}_{ext} = \bar{Z}_{ij} \Delta w_{ij} \tag{2.36}$$

For equilibrium in the radial direction

$$W^{w}_{ext} + W^{w}_{int} = 0 \tag{2.37}$$

Thus, the third equation representing equilibrium in the radial direction is obtained.

The complete set of equilibrium equations for typical interior points is given in Appendix A. When the equilibrium equations for all grid points in the model are formulated, they constitute a set of linear algebraic simultaneous equations in terms of the three displacements. These equations are mathematically consistent with the finite difference expressions of the bending theory of a general shell. If one radius of curvature is infinite, the equations are those for a cylinder [16]. If both radii are infinite, the plate equations result [1].

BOUNDARY CONDITIONS

3.1. General

One of the advantages of using models to study the behavior of shell structures is their adaptability to various boundary conditions. As was mentioned in Section 2.7, the internal work of the system corresponding to a virtual displacement can be formulated in terms of strains, Eqs. (2.29 and 2.35). Since the geometric and the force boundary conditions can be expressed by strain-displacement relations, the internal work of the deformable nodes on or near the boundary is easily obtained by the use of appropriate strains. The procedure for obtaining the equilibrium equations of points on or near the boundary is similar to the procedure for obtaining the equilibrium equations of typical interior points, i.e. the desired point is given a virtual displacement and the sum of the internal and the external works of the system associated with the virtual displacement is set equal to zero.

Whenever the strain-displacement relations at the deformable nodes on or near the boundary include displacements of points outside the model, new strain-displacement relations must be formulated. These expressions are obtained according to the restraints at the edge and include only displacements of points within the model.

3.2. Simply Supported Edge

3.2.1. Roller Support

This type of support, usually referred to as "diaphragm support" is rigid in its plane but offers no resistance in the direction normal to the plane. Assuming that the edge parallel to the y-axis is supported by rollers,

the following conditions must be satisfied:

$$\begin{aligned} v &= 0 \\ w &= 0 \\ N_x &= 0 \\ M_x &= 0 \end{aligned} \tag{3.1}$$

With the above relations, the strains at the deformable nodes on or near the edge can be easily formulated.

Node on the edge. Using the first two conditions of Eqs. (3.1), the extensional and the flexural strains in the y direction at the deformable node ij located on the edge are obtained from Eqs. (2.5 and 2.13).

$$\begin{aligned} \epsilon_{yij} &= 0 \\ \chi_{yij} &= 0 \end{aligned} \tag{3.2}$$

Using the last two conditions of Eqs. (3.1) and substituting ϵ_{yij} and χ_{yij} into Eqs. (2.18 and 2.24) we get

$$\begin{aligned} \epsilon_{xij} &= 0 \\ \chi_{xij} &= 0 \end{aligned} \tag{3.3}$$

Since v = 0 all along the edge, the deformable node ij cannot displace in the y direction. Thus, at the deformable node ij located on the edge, the shear strain is found to be (Fig. 11)

$$\epsilon_{xyij} = \frac{1}{L_y}(u_{ij+1} - u_{ij-1}) + \frac{2}{L_x}(-v_{i-1j}) \tag{3.4}$$

Since w = 0 all along the edge, the points of intersection of rigid bars cannot displace in the radial direction. This can be accomplished by removing the dowel pin (see Fig. 3) and rigidly connecting the two bars to

each other at the edge. The rotation of bar i-1j+1, ij+1 in the x direction (Fig. 11) can be written as

$$\theta_{xij+1} = \frac{1}{L_x/2}\left(\frac{L_x}{2R_x \cos \alpha/2}\, u_{ij+1} - \frac{1}{\cos \alpha/2}\, w_{i-1j+1}\right) \tag{3.5}$$

Similarly, the rotation of bar i-1j-1, ij-1 in the x direction is

$$\theta_{xij-1} = \frac{1}{L_x/2}\left(\frac{L_x}{2R_x \cos \alpha/2}\, u_{ij-1} - \frac{1}{\cos \alpha/2}\, w_{i-1j-1}\right) \tag{3.6}$$

The rotation of rigid bar i-1j-1, i-1j+1 in the y direction is

$$\theta_{yi-1j} = \frac{1}{L_y}\left[\frac{L_y}{R_y \operatorname{Cos} \beta/2}\, v_{i-1j} + \frac{1}{\operatorname{Cos} \beta/2}\left(w_{i-1j+1} - w_{i-1j-1}\right)\right] \tag{3.7}$$

The twisting strain at the deformable node ij located on the edge can now be obtained by substituting Eqs. (3.5 - 3.7) into the following relation:

$$\chi_{xyij} = \frac{1}{L_y}\left(\theta_{xij+1} - \theta_{xij-1}\right)\frac{t}{2} - \frac{1}{L_x/2}\,\theta_{yi-1j}\,\frac{t}{2} \tag{3.8}$$

Thus,

$$\begin{aligned}\chi_{xyij} = {} & \frac{t}{2R_x L_y \operatorname{Cos} \alpha/2}\left(u_{ij+1} - u_{ij-1}\right) + \frac{t}{2R_y L_x \operatorname{Cos} \beta/2}\left(-2v_{i-1j}\right) \\ & + \frac{t}{2L_x L_y}\left(\frac{1}{\operatorname{Cos} \alpha/2} + \frac{1}{\operatorname{Cos} \beta/2}\right)\left(-2w_{i-1j+1} + 2w_{i-1j-1}\right)\end{aligned} \tag{3.9}$$

Node one-half space from the edge. The strain expressions ϵ_{xij}, ϵ_{yij}, and χ_{yij} at the deformable node ij located one-half space from the edge are similar to those of a typical interior node. The shear strain ϵ_{xyij} and the twisting strain χ_{xyij} are obtained by substituting Eqs. (3.1) into Eqs. (2.8 and 2.15). Thus,

$$\epsilon_{xyij} = \frac{1}{L_y}(u_{ij+1} - u_{ij-1}) + \frac{1}{L_x}(-v_{i-1j}) - 2\frac{d}{L_x L_y} w_{ij}$$

$$\chi_{xyij} = \frac{t}{2R_x L_y \cos \alpha/2}(u_{ij+1} - u_{ij-1}) + \frac{t}{2R_y L_x \cos \beta/2}(-v_{i-1j}) \qquad (3.10)$$

$$+ \frac{t}{2L_x L_y}\left(\frac{1}{\cos \alpha/2} + \frac{1}{\cos \beta/2}\right)(-w_{i-1j+1} + w_{i-1j-1})$$

The flexural strain χ_{xij} is obtained by substituting expressions similar to Eqs. (2.10 and 3.5) into Eq. (2.11). Therefore,

$$\chi_{xij} = \frac{t}{2R_x L_x \cos \alpha/2}(u_{i+1j} - u_{i-1j}) + \frac{t}{2L_x^2 \cos \alpha/2}(-3w_{ij} + w_{i-2j}) \qquad (3.11)$$

Node one space from the edge. At the deformable node ij located one space from the edge, all strains except χ_x are similar to those of a typical interior node. The flexural strain χ_{xij} is

$$\chi_{xij} = \frac{t}{2R_x L_x \cos \alpha/2}(u_{i+1j} - u_{i-1j}) + \frac{t}{2L_x^2 \cos \alpha/2}(-2w_{ij} + w_{i-2j}) \qquad (3.12)$$

Equilibrium equations. The equilibrium equations for points on or near the edge can now be obtained by the principle of virtual displacement. For example, to obtain the equilibrium equation in the y direction at point ij+1 located one-half space from the edge, the point is given a virtual displacement Δv_{ij+1}. The internal work of the system is thus given by

$$W^v_{int} = -\frac{Eh}{1-\nu^2}\frac{L_x L_y}{2}\Big[(\epsilon_{yij} + \nu\epsilon_{xij})\Delta\epsilon_{yij} + (\chi_{yij} + \nu\chi_{xij})\Delta\chi_{yij}$$

$$+ (\epsilon_{yij+2} + \nu\epsilon_{xij+2})\Delta\epsilon_{yij+2} + (\chi_{yij+2} + \nu\chi_{xij+2})\Delta\chi_{yij+2}$$

$$+ \frac{1-\nu}{2}(\epsilon_{xyi-1j+1}\,\Delta\epsilon_{xyi-1j+1} + \chi_{xyi-1j+1}\,\Delta\chi_{xyi-1j+1}$$

$$+ \frac{1}{2}\epsilon_{xyi+1j+1}\,\Delta\epsilon_{xyi+1j+1} + \frac{1}{2}\chi_{xyi+1j+1}\,\Delta\chi_{xyi+1j+1})\Big] \qquad (3.13)$$

The coefficient 1/2 which appears in the last two terms of Eq. (3.13) is due to the reduced width of the strip of the shell at the edge, Fig. 11. The external work of the system is

$$W^{v}_{ext} = \bar{Y}_{ij+1}\, \Delta v_{ij+1} \tag{3.14}$$

For equilibrium

$$W^{v}_{ext} + W^{v}_{int} = 0 \tag{3.15}$$

Substituting the appropriate strain-displacement relations into Eq. (3.13) and then substituting the result and Eq. (3.14) into Eq. (3.15), the desired equilibrium equation is obtained. Thus,

$$\begin{aligned}
&\frac{L_x L_y}{2}\Bigg[\left(\frac{1}{\cos^2\beta/2} + \frac{t^2}{4R_y^2\cos^2\beta/2}\right)\frac{1}{L_y^2}\left(v_{ij+3} - 2v_{ij+1} + v_{ij-1}\right)\\
&+ \frac{1-\nu}{2}\left(1 + \frac{t^2}{4R_y^2\cos^2\beta/2}\right)\frac{1}{L_x^2}\left(-3v_{ij+1} + v_{i-2j+1}\right) + \left(\frac{1-\nu}{2} + \frac{\nu}{\cos\alpha/2\cos\beta/2}\right.\\
&\left.+ \frac{1+\nu}{2}\,\frac{t^2}{4R_xR_y\cos\alpha/2\cos\beta/2}\right)\frac{1}{L_xL_y}\left(u_{i+1j+2} - u_{i-1j+2} - u_{i+1j} + u_{i-1j}\right)\\
&- \left(\frac{1}{R_y\cos\beta/2} + \frac{\nu}{R_x\cos\alpha/2\cos\beta/2}\right)\frac{1}{L_y}\left(w_{ij+2} - w_{ij}\right) - \left(\frac{1-\nu}{L_xL_y}\right)\frac{d}{L_x}\left(-w_{i-1j+1}\right)\\
&+ \left(\frac{t^2}{4R_y\cos^2\beta/2}\right)\frac{1}{L_y^3}\left(w_{ij+4} - 3w_{ij+2} + 3w_{ij} - w_{ij-2}\right)\\
&+ \frac{t^2}{4R_y\cos\beta/2}\left(\frac{1-\nu}{2}\,\frac{1}{\cos\beta/2} + \frac{1+\nu}{2}\,\frac{1}{\cos\alpha/2}\right)\frac{1}{L_x^2L_y}\left(-3w_{ij+2} + w_{i-2j+2}\right.\\
&\left.+ 3w_{ij} - w_{i-2j}\right)\Bigg] + \frac{1-\nu^2}{Eh}\,\bar{Y} = 0
\end{aligned} \tag{3.16}$$

3.2.2. Hinge Support

The difference between the hinge support and the roller support is that the former cannot move in a direction perpendicular to the edge. Therefore, the boundary conditions, when the edge parallel to the y axis is hinge supported, are

$$\begin{aligned} u &= 0 \\ v &= 0 \\ w &= 0 \\ M_x &= 0 \end{aligned} \tag{3.17}$$

Taking these conditions into account the strains at the deformable nodes on or near the edge are obtained and the equilibrium equations for displacement points near the edge are formulated. The procedure is similar to that of roller support.

3.3. Free Edge

Assuming that the edge parallel to the y axis is completely free, the boundary conditions are

$$\begin{aligned} N_x &= 0 \\ N_{xy} &= 0 \\ M_x &= 0 \\ R_x &= 0 \end{aligned} \tag{3.18}$$

where R_x is the classical reaction composed of the shear force Q and the variation of the twisting moment M_{xy} along the edge, i.e.

$$R_x = Q_x + \frac{\partial M_{xy}}{\partial y} = Q_x + Q_x' \tag{3.19}$$

Since the classical shell theory is used as a guide in the development of the model, the reaction R_x must be defined at points along the edge which best simulate a behavior similar to the continuous shell. The most logical points are the points of intersections of rigid bars along the edge. For example, the reaction at point ij+1, Fig. 12, is composed of the shear force Q_{xij+1} which results from the bending moment $M_{xi-1j+1}$, and Q'_{xij+1} which results from the two adjacent twisting moments M_{xyij} and M_{xyij+2}.

As was pointed out in Section 2.2, at the points of crossings of the rigid bars, the two bars displace independently of each other in the radial direction. Therefore, the forces Q' resulting from the twisting moments along the edge must be transferred to the ends of the bars intersecting the edge. This is accomplished by means of auxiliary rigid bars (Fig. 12) which connect the nodes on the edge to the points on the edge where the bars cross. To eliminate any additional twisting moment at the nodes one-half space from the edge which may result from the displacements of nodes along the edge, frictionless hinges are inserted at points of connections of auxiliary rigid bars and the crossing bars.

By the use of Eqs. (3.18), the strains of the deformable nodes on or near the free edge can be easily formulated.

Node on the edge. Since the strain-displacement expressions are geometric relations, both the extensional and the flexural strains in the y direction at the deformable node ij located on the edge are similar to those of a typical interior node, Eqs. (2.5 and 2.13). The expressions for the extensional and the flexural strains in the x direction at the deformable node ij located on the edge are obtained from the first and the third of Eqs. (3.18). Thus,

$$\epsilon_{xij} = -\nu \left[\frac{1}{L_y \cos \beta/2} (v_{ij+1} - v_{ij-1}) - \frac{1}{R_y \cos \beta/2} w_{ij} \right] \tag{3.20}$$

$$\chi_{xij} = -\nu \left[\frac{t}{2R_y L_y \cos \beta/2} (v_{ij+1} - v_{ij-1}) + \frac{t}{2L_y^2 \cos \beta/2} (w_{ij+2} - 2w_{ij} + w_{ij-2}) \right] \tag{3.21}$$

At the deformable node ij located on the edge, the shear strain is found from the second of Eqs. (3.18) to be

$$\epsilon_{xyij} = 0 \tag{3.22}$$

To obtain the twisting strain, we first have to consider the rotation of rigid bars i-1j+1, ij+1 and i-1j-1, ij-1. The location of these bars is as shown in Fig. 13. Since at the crossing points on the edge, the two bars displace in the radial direction independently of each other, additional unknowns, δ's (radial displacements of the ends of the crossing bars), are introduced. Additional equations necessary to solve for the extra unknown δ's are formulated later from the equilibrium of a portion of the model near the edge. With the extra unknown δ's, the rotation of bar i-1j+1, ij+1 in the x direction is (see Fig. 14a)

$$\theta_{xij+1} = \frac{1}{L_x/2} \left(\delta_{ij+1} - \frac{1}{\cos \alpha/2} w_{i-1j+1} + \frac{L_x}{2R_x \cos \alpha/2} u_{ij+1} \right) \tag{3.23}$$

Similarly the rotation of bar i-1j-1, ij-1 in the x direction is

$$\theta_{xij-1} = \frac{1}{L_x/2} \left(\delta_{ij-1} - \frac{1}{\cos \alpha/2} w_{i-1j-1} + \frac{L_x}{2R_x \cos \alpha/2} u_{ij-1} \right) \tag{3.24}$$

The rotation of rigid bar i-2j, ij (which is equal to the y rotation of bar i-1j-1, i-1j+1) in the y direction is

$$\theta_{yi-1j} = \frac{1}{L_y}\left[\frac{L_y}{R_y \cos \beta/2} v_{i-1j} + \frac{1}{\cos \beta/2}(w_{i-1j+1} - w_{i-1j-1})\right] \tag{3.25}$$

The rotations of the two auxiliary rigid bars ij-1, ij and ij, ij+1 in the y direction are

$$\begin{aligned}\theta^1_{ij} &= \frac{1}{L_y/2}\left(\frac{1}{\cos \beta/2} w_{ij} + \frac{L_y}{2R_y \cos \beta/2} v_{ij} - \delta_{ij-1}\right)\\ \theta^2_{ij} &= \frac{1}{L_y/2}\left(\delta_{ij+1} - \frac{1}{\cos \beta/2} w_{ij} + \frac{L_y}{2R_y \cos \beta/2} v_{ij}\right)\end{aligned} \tag{3.26}$$

respectively. The displacement v_{ij} of the node ij in the y direction is equal to v_{i-1j}. The average rotation at the node ij is

$$\theta_{yij} = \frac{1}{2}(\theta^1_{ij} + \theta^2_{ij}) = \frac{1}{L_y}\left[\frac{L_y}{R_y \cos \beta/2} v_{ij} + (\delta_{ij+1} - \delta_{ij-1})\right] \tag{3.27}$$

The twisting strain is defined by

$$\chi_{xyij} = \frac{1}{L_y}(\theta_{xij+1} - \theta_{xij-1})\frac{t}{2} + \frac{1}{L_x/2}(\theta_{yij} - \theta_{yi-1j})\frac{t}{2} \tag{3.28}$$

Substituting Eqs. (3.23, 3.24, 3.25, and 3.27) into Eq. (3.28) yields

$$\begin{aligned}\chi_{xyij} = {} & \frac{t}{2R_x L_y \cos \alpha/2}(u_{ij+1} - u_{ij-1}) + \frac{t}{2L_x L_y}\left(\frac{1}{\cos \alpha/2}\right.\\ & \left. + \frac{1}{\cos \beta/2}\right)(-2w_{i-1j+1} + 2w_{i-1j-1}) + \frac{2t}{L_x L_y}(\delta_{ij+1} - \delta_{ij-1})\end{aligned} \tag{3.29}$$

Node one-half space from the edge. At the deformable node ij located one-half space from the edge, all strains except χ_x are similar to those of a typical interior node. The flexural strain χ_{xij} is obtained from expressions similar to Eqs. (2.10, 2.11 and 3.23). Thus,

$$\chi_{xij} = \frac{t}{2R_x L_x \cos \alpha/2} (u_{i+1j} - u_{i-1j}) + \frac{t}{2L_x^2 \cos \alpha/2} (-3w_{ij} + w_{i-2j})$$

$$+ \frac{t}{L_x^2} \delta_{i+1j} \tag{3.30}$$

Considering the equilibrium of a T section near the edge, Fig. 14b, the following relations can be written:

$$Q_{xij+1} = \frac{1}{L_x/2} M_{xi-1j+1}$$

$$Q'_{1xij+1} = \frac{1}{L_y/2} M_{xyij} \tag{3.31}$$

$$Q'_{2xij+1} = \frac{1}{L_y/2} M_{xyij+2}$$

where

$$M_{xi-1j+1} = - \frac{Eh}{1-\nu^2} \frac{L_y}{2} \frac{t}{2} (\chi_{xi-1j+1} - \nu \chi_{yi-1j+1})$$

$$M_{xyij} = - \frac{Eh}{2(1+\nu)} \frac{L_y}{2} \frac{t}{2} \chi_{xyij} \tag{3.32}$$

$$M_{xyij+2} = - \frac{Eh}{2(1+\nu)} \frac{L_y}{2} \frac{t}{2} \chi_{xyij+2}$$

For the equilibrium in vertical direction

$$Q_{xij+1} + Q'_{2xij+1} - Q'_{1xij+1} = 0 \tag{3.33}$$

Substituting Eqs. (3.32) into Eqs. (3.31) and then substituting the results into Eq. (3.33), we obtain

$$\frac{L_y}{L_x} (\chi_{xi-1j+1} + \nu \chi_{yi-1j+1}) + \frac{1-\nu}{2} (\chi_{xyij+2} - \chi_{xyij}) = 0 \tag{3.34}$$

Equation (3.34), after substitution for strains, yields the additional equilibrium equation at the free edge. Thus,

$$\frac{L_y}{L_x}\left[\frac{1}{R_x L_x \cos\alpha/2}(u_{ij+1} - u_{i-2j+1}) + \frac{1}{L_x^2 \cos\alpha/2}(-3w_{i-1j+1} + w_{i-3j+1})\right.$$
$$+ \frac{1}{L_x^2}(2\delta_{ij+1}) + \frac{\nu}{R_y L_y \cos\beta/2}(v_{i-1j+2} - v_{i-1j}) + \frac{\nu}{L_y^2 \cos\beta/2}(w_{i-1j+3}$$
$$\left. - 2w_{i-1j+1} + w_{i-1j-1})\right] + \frac{1-\nu}{2}\left[\frac{1}{R_x L_y \cos\alpha/2}(u_{ij+3} - 2u_{ij+1} + u_{ij-1})\right.$$
$$+ \frac{1}{R_y L_x \cos\beta/2}(-2v_{i-1j+2} + 2v_{i-1j}) + \frac{1}{L_x L_y}\left(\frac{1}{\cos\alpha/2} + \frac{1}{\cos\beta/2}\right)(-2w_{i-1j+3}$$
$$\left. + 4w_{i-1j+1} - 2w_{i-1j-1}) + \frac{1}{L_x L_y}(4\delta_{ij+3} - 8\delta_{ij+1} + 4\delta_{ij-1})\right] = 0 \qquad (3.35)$$

Nodes one space from the edge. At the deformable node ij located one space from the edge, all strains are similar to those of a typical interior node.

Equilibrium equations. The procedure for obtaining the equilibrium equations for points on or near the edge is similar to that of Section 3.2. For example, to obtain the equilibrium equation in the z direction at point ij on the free edge, the point is given a virtual displacement Δw_{ij}. The internal work of the system is thus given by

$$W_{int}^{w} = -\frac{Eh}{1-\nu^2}\frac{L_x L_y}{2}\left[(\epsilon_{xi-2j} + \nu\epsilon_{yi-2j})\Delta\epsilon_{xi-2j} + (\chi_{xi-2j} + \nu\chi_{yi-2j})\Delta\chi_{xi-2j}\right.$$
$$+ \frac{1}{2}(\epsilon_{xij} + \nu\epsilon_{yij})\Delta\epsilon_{xij} + \frac{1}{2}(\chi_{xij} + \nu\chi_{yij})\Delta\chi_{xij}$$
$$\left. + \frac{1}{2}(\epsilon_{yij-2} + \nu\epsilon_{xij-2})\Delta\epsilon_{yij-2} + \frac{1}{2}(\chi_{yij-2} + \nu\chi_{xij-2})\Delta\chi_{yij-2}\right.$$

$$+ \frac{1}{2}(\epsilon_{yij} + \nu\epsilon_{xij})\,\Delta\epsilon_{yij} + \frac{1}{2}(\chi_{yij} + \nu\chi_{xij})\,\Delta\chi_{yij}$$

$$+ \frac{1}{2}(\epsilon_{yij+2} + \nu\epsilon_{xij+2})\,\Delta\epsilon_{yij+2} + \frac{1}{2}(\chi_{yij+2} + \nu\chi_{xij+2})\,\Delta\chi_{yij+2}$$

$$+ \frac{1-\nu}{2}(\epsilon_{xyi-1j-1}\,\Delta\epsilon_{xyi-1j-1} + \chi_{xyi-1j-1}\,\Delta\chi_{xyi-1j-1}$$

$$+ \epsilon_{xyi-1j+1}\,\Delta\epsilon_{xyi-1j+1} + \chi_{xyi-1j+1}\,\Delta\chi_{xyi-1j+1}$$

$$+ \frac{1}{2}\epsilon_{xyij}\,\Delta\epsilon_{xyij})\Big] \qquad (3.36)$$

The external work of the system is

$$W^{w}_{ext} = \bar{Z}_{ij}\,\Delta w_{ij} \qquad (3.37)$$

For equilibrium

$$W^{w}_{ext} + W^{w}_{int} = 0 \qquad (3.38)$$

Substituting the appropriate strain-displacement relations into Eq. (3.36) and then substituting the result and Eq. (3.37) into Eq. (3.38), the desired equilibrium equation is obtained. Thus,

$$\frac{L_x L_y}{2}\Big[-\frac{1-\nu^2}{2}\frac{1}{R_y\,\mathrm{Cos}^2\,\beta/2}\frac{1}{L_y}(v_{ij+1} - v_{ij-1}) + \frac{1-\nu^2}{2}\frac{1}{R_y^{\,2}\,\mathrm{Cos}^2\,\beta/2}w_{ij}$$

$$+ \frac{t^2}{4R_x\,\mathrm{Cos}^2\,\alpha/2}\frac{1}{L_x^{\,3}}(u_{i-1j} - u_{i-3j}) + \frac{1-\nu^2}{2}\frac{t^2}{4R_y\,\mathrm{Cos}^2\,\beta/2}\frac{1}{L_y^{\,3}}(v_{ij+3} - 3v_{ij+1}$$

$$+ 3v_{ij-1} - v_{ij-3}) + \frac{1-\nu}{2}\frac{t^2}{4R_x\,\mathrm{Cos}\,\alpha/2}\Big(\frac{1}{\mathrm{Cos}\,\alpha/2} + \frac{1}{\mathrm{Cos}\,\beta/2}\Big)\frac{1}{L_x L_y^{\,2}}(-u_{i-1j+2}$$

$$+ 2u_{i-1j} - u_{i-1j-2}) + \frac{1-\nu}{2}\frac{t^2}{4R_y\,\mathrm{Cos}\,\beta/2}\Big(\frac{1}{\mathrm{Cos}\,\alpha/2} + \frac{1}{\mathrm{Cos}\,\beta/2}\Big)\frac{1}{L_x^{\,2}L_y}(-v_{ij+1}$$

$$+ v_{i-2j+1} + v_{ij-1} - v_{i-2j-1}) + \frac{t^2}{4R_y \cos\alpha/2 \cos\beta/2} \frac{1}{L_x^2 L_y} (v_{i-2j+1}$$

$$-v_{i-2j-1}) + \frac{t^2}{4\cos^2\alpha/2} \frac{1}{L_x^4} (w_{ij} - 2w_{i-2j} + w_{i-4j}) + \frac{1-\nu^2}{2} \frac{t^2}{4\cos^2\beta/2} \frac{1}{L_y^4} (w_{ij+4}$$

$$- 4w_{ij+2} + 6w_{ij} - 4w_{ij-2} + w_{ij-4}) + \frac{1-\nu}{2} \frac{t^2}{4} \left(\frac{1}{\cos\alpha/2} + \frac{1}{\cos\beta/2}\right)^2$$

$$\frac{1}{L_x^2 L_y^2} (-w_{ij+2} + 2w_{ij} - w_{ij-2} + w_{i-2j+2} - 2w_{i-2j} + w_{i-2j-2})$$

$$+ \frac{\nu}{\cos\alpha/2 \cos\beta/2} \frac{t^2}{4} \frac{1}{L_x^2 L_y^2} (w_{i-2j+2} - 2w_{i-2j} + w_{i-2j-2})\Big] - \frac{1-\nu^2}{Eh} \bar{Z} = 0 \qquad (3.39)$$

3.4. Other Boundary Conditions

The procedure for obtaining other boundary conditions is similar to that of the simply supported and free case. For a shell clamped along the edge, all displacements and slopes along the edge vanish. For a shell continuous across a diaphragm support, the displacements vanish while the slope vanishes only if symmetrical geometry and loading conditions exist.

NUMERICAL RESULTS

4.1. General

As was mentioned previously the objective of this study is the development of a discrete model for the analysis of shallow shells of double curvature. It is not within the scope of this study to consider the effect of various parameters on the behavior of a multitude of shells. Solutions for a variety of shells with different boundary conditions are presented. One of the advantages of the discrete model is that the various types of loading can easily be handled. Several examples of shells subjected to uniform loads, sinusoidally varying distributed loads, and sinusoidally varying edge loads are given. Some solutions for shells having different values of Poisson's ratio are also presented. The obtained results are compared with existing solutions whenever possible to demonstrate the applicability of the model to a variety of shell problems.

Two types of shells are of particular interest as test problems for the model. One is a shell of negative Gaussian curvature, the hyperbolic paraboloid bounded by characteristic lines of the surface. For this shell the coordinate lines do not coincide with the lines of principal curvature. The external loads are transmitted to the supports mainly by the in-plane shear forces. The other shell of particular interest is a shell of positive Gaussian curvature, the elliptic paraboloid with two opposite edges simply supported and the other two edges free. For this shell the magnitude of N_y forces (edges parallel to the y-axis being free) varies very rapidly across a section normal to the free edges. If the model can predict the behavior of the above two shells, then it can be expected to give good estimates of

magnitude and distribution of boundary disturbances for general shell problems.

Except for the hyperbolic paraboloid bounded by the characteristic lines of the surface, the shells considered herein have both symmetrical geometry and loading. Therefore, by using only one quadrant of each shell in the analysis, one could reduce the number of unknown displacements to one-fourth of the original number. The spacing between the two extensional elements, t, is obtained by equating the bending stiffness of the model to that of the real material. Thus,

$$\frac{Eh}{1-\nu^2}\,\frac{t^2}{4} = \frac{Eh^3}{12(1-\nu^2)}$$

which gives

$$t = \frac{h}{\sqrt{3}}$$

For flat plates the equilibrium equation in the z direction, Eq. (A-3) is independent of the other two equilibrium equations, Eqs. (A-1 and A-2). Furthermore, the set of equilibrium equations in the z direction reduces to two sets of completely uncoupled equations. One set contains the w displacements of the deformable nodes marked as solid circles (see Fig. 15). The other set contains the w displacements of the deformable nodes marked as hollow circles. Although, the two systems act independently of each other, the solutions for the two sets were found to be in good agreement with one another. For example, the plot of w displacements along the diagonal of a rectangular plate is given in Fig. 16. Alternate nodes belong to one system, the remaining nodes to the other. The agreement between the two systems, as

seen from the figure, is excellent. For shells whose coordinate lines coincide with the lines of principal curvature, such as cylindrical shells, elliptic paraboloid shells, and saddle shaped hyperbolic paraboloid shells, the two sets of equations are also completely uncoupled from each other. For shells whose coordinate lines do not coincide with the lines of principal curvature, such as hyperbolic paraboloid bounded by the characteristic lines of the surface, the two sets of equations are strongly coupled through u, v, and w displacements.

4.2. All Edges Simply Supported

4.2.1. Uniformly Loaded Rectangular Plate

Two rectangular plates of same dimensions, uniformly loaded and having a Poisson's ratio of 0.3 are considered. The dimensions of the plates are given in Table 1. Because of symmetry, only one quadrant of each plate is used in the analysis. In the first plate, the quadrant is divided into three spacings in each direction. In the second plate the number of divisions in each direction is doubled. The values of the deflections and the bending moments at the center of the two plates are given in Table 1. The solutions are in good agreement with those given by Timoshenko and Woinowski-Krieger [18]. Reasonable accuracy is obtained by using a 3 x 3 grid. By increasing the number of divisions in each direction, the values of the moments are slightly improved.

4.2.2. Uniformly Loaded Cylindrical Shell

A cylindrical shell with dimensions corresponding to those given by Bouma [3] is considered. The shell is uniformly loaded and has a Poisson's

ratio of 0.0. The dimensions of the shell are given in Fig. 17. Due to symmetry only one quadrant of the shell is used in the analysis. The quadrant is divided into six spacings in each direction. The plots of the displacements w, the forces N_y, and the bending moments M_x at the midsection of the shell are also given in Fig. 17. For a modulus of elasticity of 2×10^5 kg/cm^2 and a loading of 0.019 kg/cm^2, the maximum positive and negative values of w, N_y, and M_x at the midsection of the shell are shown in Table 2. The results are compared with those given by Bouma [3]. In general the agreement is good. The small differences between the results could be due to both the manner in which the two shells are supported along the edges and the manner in which the two shells are loaded. The edges of the shell in Ref. [3] are supported by vertical diaphragms and the loading normal to the surface, is given by

$$Z(y) = Z_1 \operatorname{Cos} \alpha_1 y \tag{4.1}$$

where

$$Z_1 = \frac{4}{\pi} q \qquad , \qquad \alpha_1 = \frac{\pi}{b}$$

Although the transverse edges of the shell in this example are supported by vertical diaphragms, the longitudinal edges are supported by diaphragms which are perpendicular to the surface. The loading is considered as the weight of the shell. The most significant difference in the transverse bending moment, M_x, is to be expected because of the manner of supporting the longitudinal edges.

4.2.3. Uniformly Loaded Elliptic Paraboloid

The dimensions of the elliptic paraboloid used in this example are given in Fig. 18. The dimensions of the shell in the x direction are the same as those of the cylindrical shell, Fig. 17. The dimensions in the y direction are so chosen that the curved length and the rise of the shell are 1800 cms and 200 cms respectively. A 6 x 6 grid on a quadrant of the shell is used in the analysis. The plots of the displacements w, the forces N_y, and the bending moments M_x at the midsection of the shell are shown in Fig. 18.

Significant forces exist at the corners of this shell. The in-plane shear force and the twisting moment are

$$N_{xy} = -2.23\ qa$$

$$M_{xy} = -0.069 \times 10^{-2}\ qa^2$$

respectively. These forces produce principal stresses in the diagonal directions which are as large or larger than those which exist in the center regions of the shell.

The plots indicate that except near the edge the membrane theory provides a good estimate of stresses for design purposes. Due to low values of deflections, forces, and bending moments, this shell is very suitable for roof construction.

4.2.4. Uniformly Loaded Hyperbolic Paraboloid

The dimensions of the hyperbolic paraboloid used in this example are given in Fig. 19. The dimensions of the shell in the x direction are kept the same as those of the cylindrical and the elliptic paraboloid shells, while the dimensions in the y directions are so chosen that the curved length

and the sag of the shell are 1800 cms and 200 cms respectively. A 6x6 grid on a quadrant of the shell is used in the analysis. The plots of the displacements w, the forces N_y, and the bending moments M_x at the midsection of the shell are shown in Fig. 19.

The plots indicate that the membrane theory can not be used to estimate the stresses. The magnitudes of deflections, forces, and bending moments for this shell are much higher than those for an elliptic paraboloid and a cylindrical shell of the same dimensions.

4.2.5. Uniformly Loaded Hyperbolic Paraboloid Bounded by Characteristic Lines of the Surface

A square hyperbolic paraboloid bounded by the characteristic lines of the surface is used in this example. The shell has dimensions corresponding to those used by Chetty and Tottenham [5]. The dimensions of the shell are given in Fig. 20. The Poisson's ratio and the modulus of elasticity of the shell are 0.16 and 3×10^6 psi respectively. The shell is subjected to a uniform load of 50 lbs/ft^2. Since the shell is not symmetric, an 8x8 grid on the complete shell is used in the analysis. The plots of deflection w, the force N_{xy}, and the bending moment M_x at the midsection of the shell as obtained with the model together with the corresponding values obtained by Chetty and Tottenham are shown in Fig. 20. The agreement between the deflections and the shear forces is very good while the maximum bending moment obtained by the model is slightly higher than the one in Ref. [5].

As was mentioned previously, this shell is of particular interest in the test of the model. The results indicate that the model can indeed be used to study the behavior of shells of negative Gaussian curvature.

4.3. Two Opposite Edges Simply Supported and the Remaining Two Edges Free

4.3.1. Uniformly Loaded Square Plate

A square plate uniformly loaded and having a Poisson's ratio of 0.3 is considered. The dimensions of the plate are given in Table 3. A 5x5 grid on a quadrant of the plate is used in the analysis. The values of the deflections and the bending moments at the center and at the free edge of the plate are given in Table 3. The results are in good agreement with those given by Timoshenko and Woinowsky-Krieger [18].

4.3.2. Cylindrical Shell Subjected to Sinusoidally Varying Edge Load

A cylindrical shell with the transverse edges supported by diaphragms and the longitudinal edges free is considered in this example. The dimensions of the shell are given in Fig. 21. The Poisson's ratio and the modulus of elasticity of the shell are 0.15 and 4.32×10^5 kips/ft^2 respectively. The shell is loaded along its longitudinal edges by a loading of the type

$$Z(y) = \text{Cos} \frac{\pi}{b} y$$

A quadrant of the shell is divided into 10 and 6 spacings in the x and y directions respectively. The plots of displacements w, the forces N_y, and the bending moments M_x at the midsection of the shell are shown in Fig. 21. The analytical solution which was obtained by a Fourier series solution of the differential equation is taken from Parikh [15]. The fact that the results are in good agreement with the analytical solution indicates that the model can be used to study the effect of edge disturbances in shells. Parikh's model, which is an extension of Hrennikoff's framework [12] to cylindrical shells, does not demonstrate the same accuracy as the model presented in this

the displacements w, the forces N_y, and the bending moments M_x at the mid-section of the shell are also shown in Fig. 22. The plots of the in-plane shear forces N_{xy} and the forces N_y at the support for the two shells are given in Fig. 23.

The magnitudes of w, N_y, and M_x at the midsection of the shell having hinged support are lower than those of the shell having roller support. The magnitudes of N_{xy} and N_y at the hinged support are much higher than those at the roller support. This is to be expected in view of the fact that the shell now behaves in a manner like a fixed ended beam. However, as pointed out below computations based on considering the shell as a fixed beam are not adequate.

A comparison of the hinged support case with the stresses that are obtained by multiplying the N_y stresses for the roller case by the ratio of the bending moment in a fixed ended beam to the center moment in a simply supported beam is not conservative. The error also may not be insignificant. Furthermore, the substantial modification of the N_{xy} stress distriabution is not predicted by such an approximation.

The equilibrium of the model is checked by considering one-half of the shell and applying the usual equilibrium equations. The summations of the forces in the horizontal and the vertical directions vanish and the summation of the moments about any axis is found to be zero, i.e. the internal forces produce moments equal and opposite to the simple beam moment $1/8\ wL^2$.

4.3.4. Elliptic Paraboloid Subjected to Sinusoidally Varying Load

The dimensions of the elliptic paraboloid shells used in this example are similar to those of the simply supported case and are given in

reaction of 0.95 qa which is 1.7 percent of the N_y force at the free edge. Reducing the value of the N_y force at the free edge, obtained from the model, by 1.7 percent gives a N_y equal to 2102 kg/cm. As was mentioned previously, this shell is of particular interest in the test of the model. The results indicate that the model can be used to predict the rapid variation in forces and bending moments.

Due to large values of deflections, forces, and bending moments and also due to rapid variation of N_y forces, this shell is not an ideal shell for construction.

4.3.5. Hyperbolic Paraboloid Subjected to Sinusoidally Varying Load

The dimensions of the hyperbolic paraboloid considered in this example are similar to those of the simply supported case, and are given in Fig. 27. The shell has a Poisson's ratio of 0.0 and is subjected to a loading of the type

$$Z(y) = q \cos \frac{\pi}{b} y$$

A 12x6 grid on a quadrant of the shell is used in the analysis. The plots of the displacements w, the forces N_y, and the bending moments M_x at the midsection of the shell are given in Fig. 27. The magnitude of the displacement at the free edge is very small which indicates a behavior somewhat similar to that of the simply supported case.

CONCLUSIONS AND RECOMMENDATIONS FOR FURTHER STUDIES

5.1. Conclusions

The discrete model developed in this study can be used to analyze a variety of shallow shells. The model gives good estimates of the magnitude and the distribution of deflections and stresses in shells with different edge conditions, different types of loading, and different values of Poisson's ratio. The comparisons of results indicate that the model can be used to study the behavior of shells of different Gaussian curvatures. It can also be used to study the effect of edge disturbances in shells. Rapid variations in forces and moments through the shell can be predicted by the model, however, for better results larger number of spacings should be used. In general, the obtained results are sufficiently accurate for design purposes.

In view of the construction of the deformable nodes and the existance of constant forces across each node, an approximate analysis which includes the plastic behavior is possible. Partial loadings and the extension of the model to include elastic supports, columns or point supports along the edge, different material properties at different nodes, and shells with variable thickness should not present any difficulty.

For elastic shells whose coordinate lines coincide with the lines of principal curvature, the model can be reduced to the one in Ref. [16]. The extensional and the flexural behavior are then defined at the nodes of every other row, while the shear and the twisting behavior are defined at the remaining nodes. Radial displacements are specified at the extensional nodes, and only one tangential displacement is needed at each intersection

of two rigid bars. The number of equations are thus reduced to one-half, permitting an increase in the number of spacings in the two directions.

Although the method of analysis is straightforward, the equilibrium equations governing the behavior of the model are very complex. An efficient method of computation which eliminates the possibility of human errors is to generate and solve the equilibrium equations within a digital computer. With such a computer program for the model it is possible to ecconomically investigate a variety of loading cases and support conditions which are encountered in the construction of shell roofs.

5.2. Recommendations for Further Studies

In future studies, the behavior of a portion of the model subjected to a complete set of edge disturbances should be investigated. The analysis of non-shallow shells, continuous shells, different combinations of hyperbolic paraboloid units which are bounded by the characteristic lines of the surface, and finally arch dams can then proceed by proper combinations of various portions.

The model should be extended to include elastic supports, so that the behavior of shells with edge beams or supported by columns could be investigated.

The governing equations of the model should be modified to include generalized α's and β's. Solutions of shells with variable curvatures such as elliptic and parabolic cylinders and conoids can then be easily obtained. The model should be generalized to non-orthogonal coordinates, so that shells which cover a non-rectangular planforms could be considered.

Finally, the application of the model to non-linear problems in shells should be investigated.

BIBLIOGRAPHY

1. Ang, A. H. S. and Newmark, N. M., "A Numerical Procedure for the Analysis of Continuous Plates," Proceedings of the Second American Society of Civil Engineers Conference on Electronic Computation, Pittsburg, Pennsylvania, September 1960.

2. Benard, E. F., "A Study of the Relationship Between Lattice and Continuous Structures," Ph.D. Thesis, University of Illinois, September 1965.

3. Bouma, A. L., "Some Applications of the Bending Theory Regarding Doubly Curved Shells," Proceedings of the Symposium on the Theory of Thin Elastic Shells, August 1959.

4. Bouma, A. L., "On Approximate Methods of Shell Analysis: A General Survey," Proceedings of World Conference on Shell Structure, San Francisco, California, October 1962.

5. Chetty, S. M. K. and Tottenham, H., "An Investigation into the Bending Analysis of Hyperbolic Paraboloid Shells," Indian Concrete Journal, July 1964.

6. Chuang, K. P. and Veletsos, A. S., "A Study of Two Approximate Methods of Analyzing Cylindrical Shell Roofs," Civil Engineering Studies, Structural Research Series No. 258, University of Illinois, October 1962.

7. Clough, R. W., "The Finite Element Method in Plane Stress Analysis," Proceedings of the Second American Society of Civil Engineers Conference on Electronic Computation, Pittsburgh, Pennsylvania, September 1960.

8. Clough, R. W. and Tocher, J. L., "Analysis of Thin Arch Dams by Finite Element Method," International Symposium on the Theory of Arch Dams, Southampton University, Pergamon Press, 1964.

9. Das Gupta, N. C., "Using Finite Difference Equations to Find the Stresses in Hypar Shells," Civil Engineering and Public Works Review, February 1961.

10. Das Gupta, N. C., "Edge Disturbances in a Hyperbolic Paraboloid," Civil Engineering and Public Works Review, February 1963.

11. Design of Cylindrical Concrete Shell Roofs, American Society of Civil Engineers, Manuals of Engineering Practice, No. 31, adopted 1951.

12. Hrennikoff, A., "Solution of Problems in Elasticity by Framework Method," Journal of Applied Mechanics, Vol. 8, No. 4, December 1941.

13. Langhaar, H. L., "Foundation of Practical Shell Analysis," Department of Theoretical and Applied Mechanics, University of Illinois, June 1964.

14. Noor, A. K., "Analysis of Doubly Curved Shells," Ph.D. Thesis, University of Illinois, August 1963.

15. Parikh, K. S., "Analysis of Shells Using Framework Analogy," Sc.D. Thesis, Massachusetts Institute of Technology, June 1962.

16. Schnobrich, W. C., "A Physical Analogue for the Analysis of Cylindrical Shells," Ph.D. Thesis, University of Illinois, June 1962.

17. Soare, M., Application des Equations aux Differences Finies au Calcul des Coques, Editions de L'Academie de la Republique Populaire Roumaine, Bucarest, 1962.

18. Timoshenko, S. and Woinowsky-Krieger, S., Theory of Plates and Shells, McGraw-Hill Book Company, New York, 1949.

19. Yettram, A. L. and Husain, H. M., "Grid-Framework Method for Plates in Flexure," Proceedings of the American Society of Civil Engineers, June 1965.

20. Zienkiewicz, O. C. and Cheung, Y. K., "The Finite Element Method for Analysis of Elastic, Isotropic and Orthotropic Slabs," Proceedings of the Institution of Civil Engineers, August 1964.

21. Zienkiewicz, O. C. and Cheung, Y. K., "Finite Element Method of Analysis of Arch Dam Shells and Comparison with Finite Difference Procedures," International Symposium on the Theory of Arch Dams, Southampton University, Pergamon Press, 1964.

TABLE 1. SOLUTION OF SIMPLY SUPPORTED RECTANGULAR PLATE

a = 6.0"

b = 7.2"

h = 0.03"

ν = 0.3

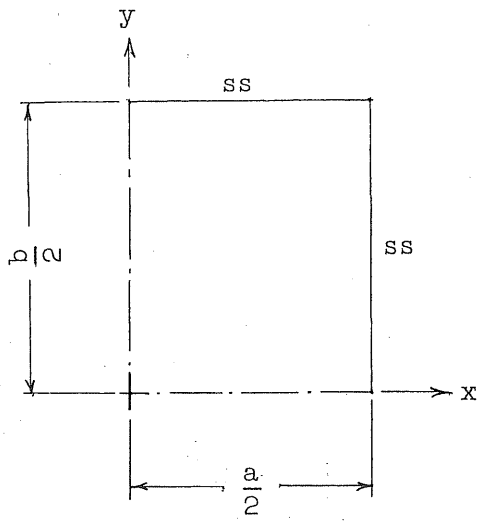

Method	x = 0 , y = 0		
	w qa^4/D	M_x qa^2	M_y qa^2
Model 3x3	0.00563	0.0613	0.0491
Model 6x6	0.00564	0.0623	0.0498
Ref. [18]	0.00564	0.0627	0.0501

TABLE 2. MAXIMUM POSITIVE AND NEGATIVE VALUES OF w, N_y, AND M_x AT THE MIDSECTION OF SIMPLY SUPPORTED CYLINDRICAL SHELL

$E = 2 \times 10^5$ kg/cm^2 , $q = 0.019$ kg/cm^2

	w , cm		N_y , kg/cm		M_x , kg	
	Pos.	Neg.	Pos.	Neg.	Pos.	Neg.
Model	0.61	-0.22	No Pos. Value	-67.8	153.0	-90.2
Ref.[b] [3]	0.60	Not Given	No Pos. Value	-63.6	163.7	-119.1

TABLE 3. SOLUTION OF SQUARE PLATE, TWO OPPOSITE EDGES SIMPLY SUPPORTED, THE OTHER TWO EDGES FREE

a = 5.0"

h = 0.03"

ν = 0.3

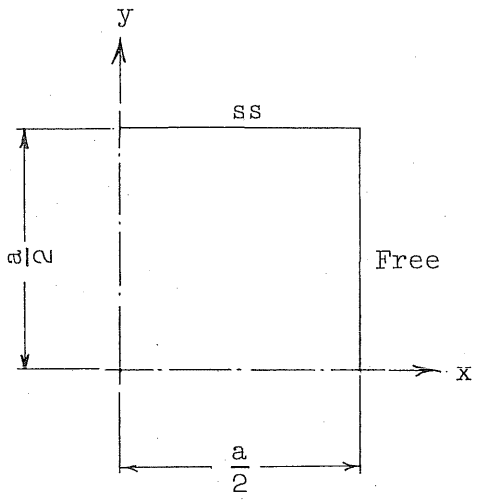

Method	x = 0 , y = 0			x = a/2 , y = 0	
	w qa^4/D	M_x qa^2	M_y qa^2	w qa^4/D	M_y qa^2
Model 5x5	0.01320	0.0269	0.1225	0.01511	0.1309
Ref. [18]	0.01309	0.0271	0.1225	0.01509	0.1318

TABLE 4. MAXIMUM POSITIVE AND NEGATIVE VALUES OF w, N_y, AND M_x AT THE MIDSECTION OF CYLINDRICAL SHELL, TWO OPPOSITE EDGES SIMPLY SUPPORTED, THE OTHER TWO EDGES FREE

$E = 2 \times 10^5$ kg/cm^2 , $q = 0.019$ kg/cm^2

	w , cm		N_y , kg/cm		M_x , kg	
	Pos.	Neg.	Pos.	Neg.	Pos.	Neg.
Model	14.2	-2.3	858.7	-242.3	--	-498.2
Ref. [3]	32.0	Not given	875.0	-225.0	--	-500.0

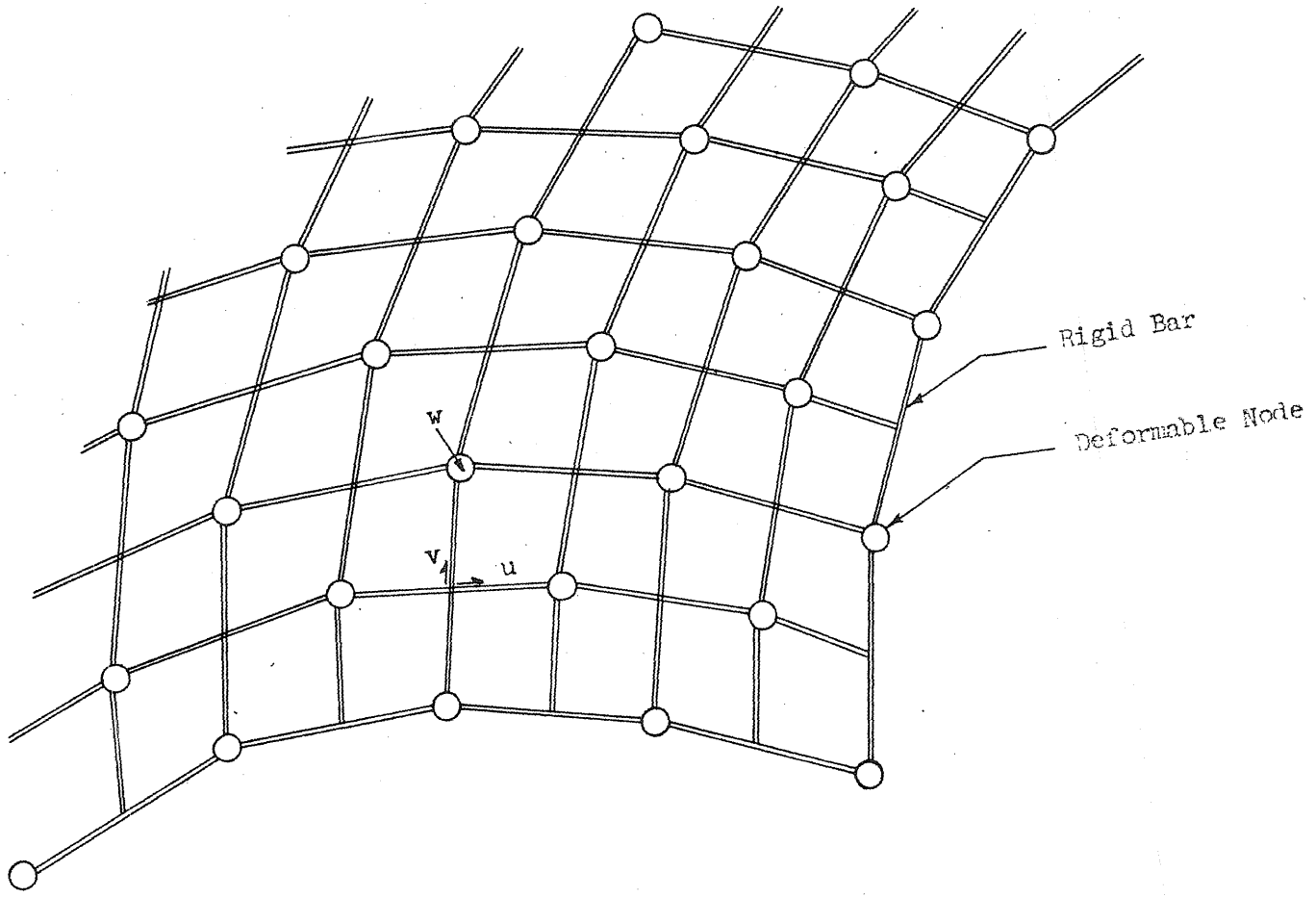

FIG. 1 TYPICAL MODEL OF POSITIVE CURVATURE

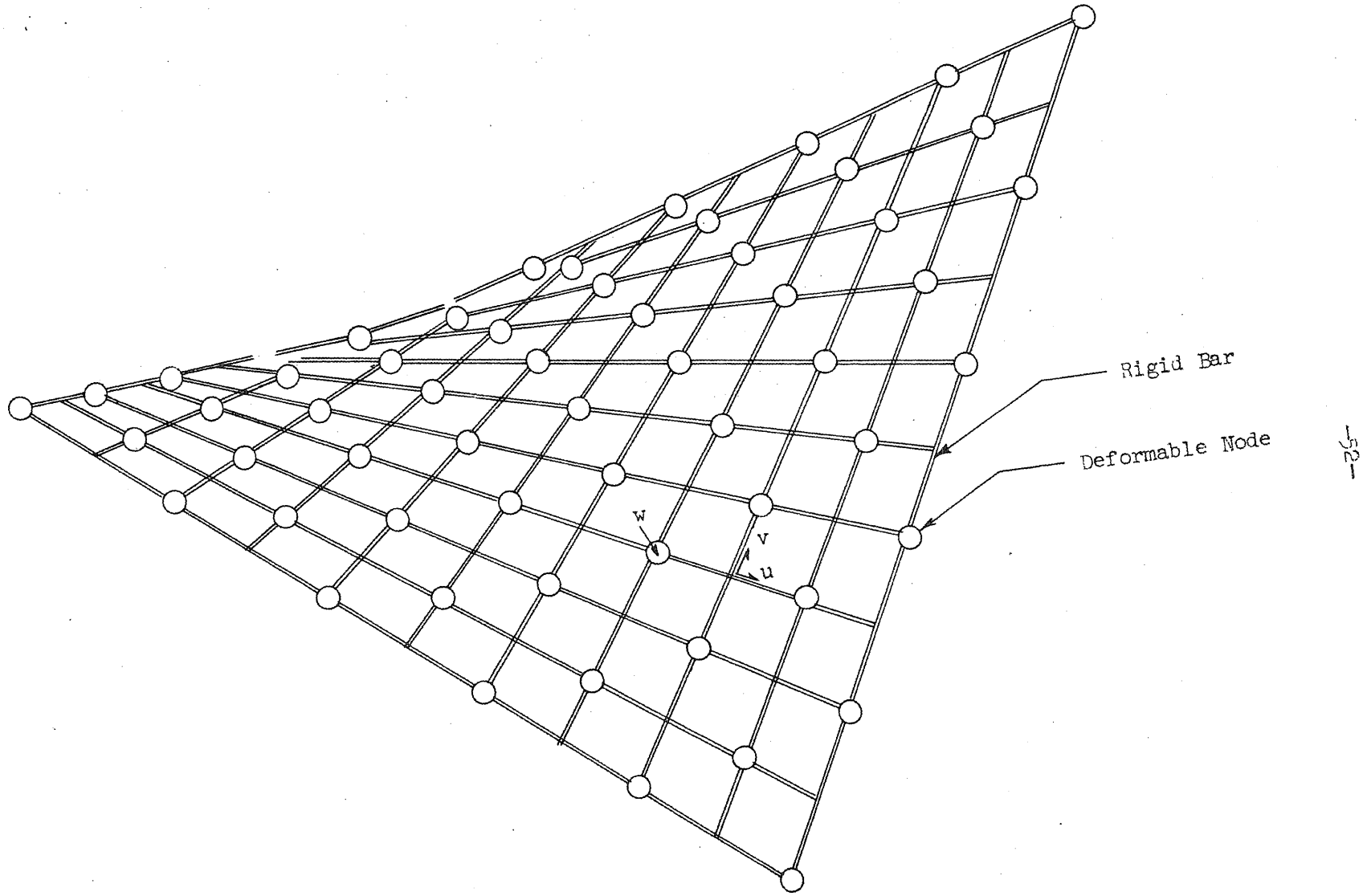

FIG. 2 TYPICAL MODEL OF NEGATIVE CURVATURE

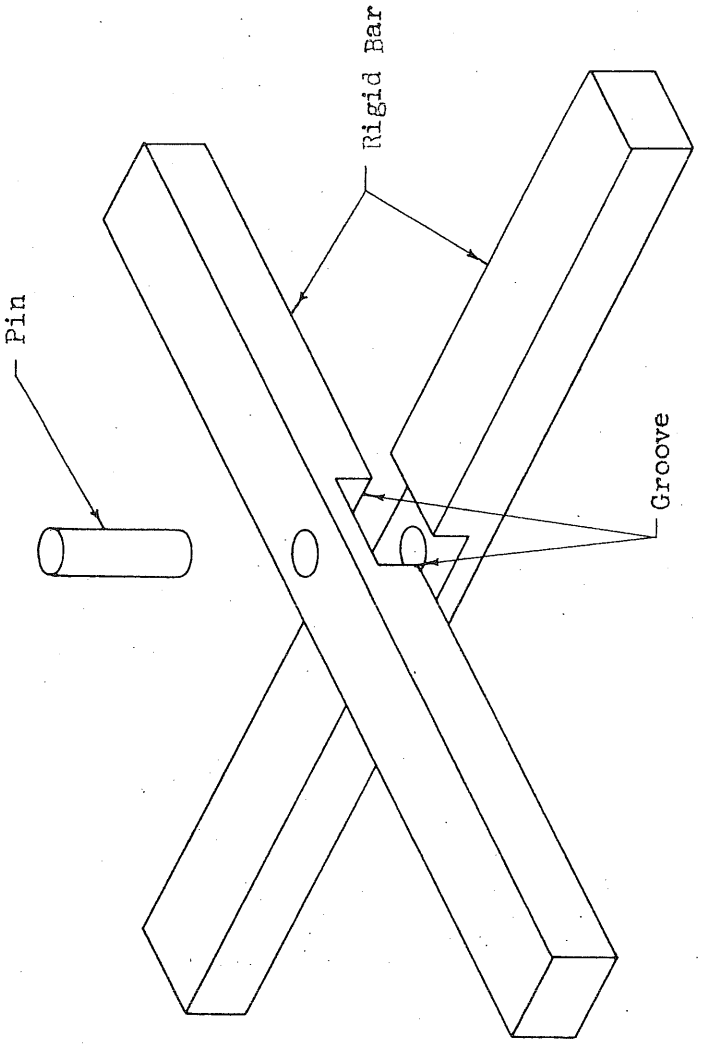

FIG. 3 RIGID JOINT CONNECTION

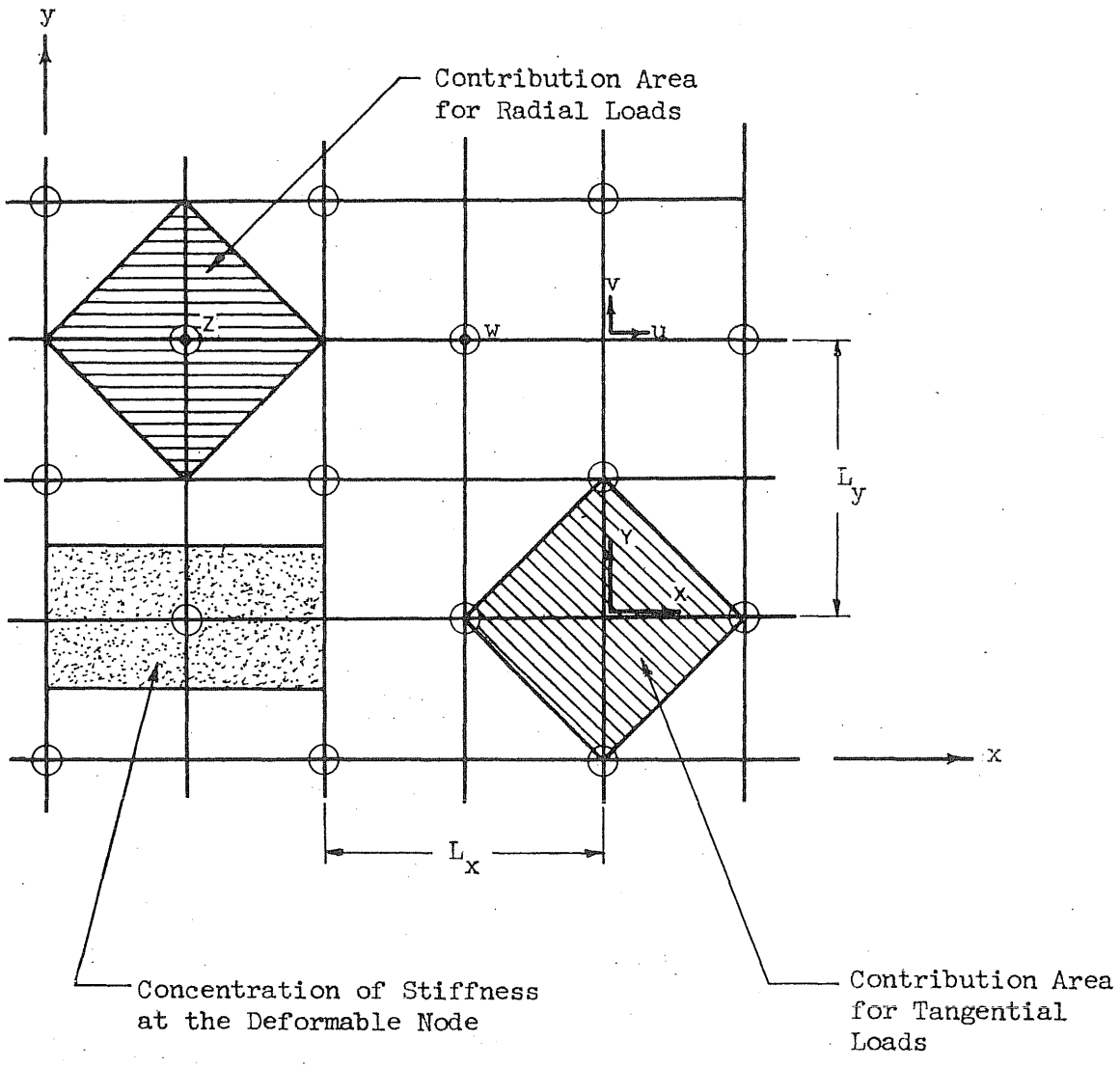

FIG. 4 LOCATIONS OF DISPLACEMENTS AND LOADS

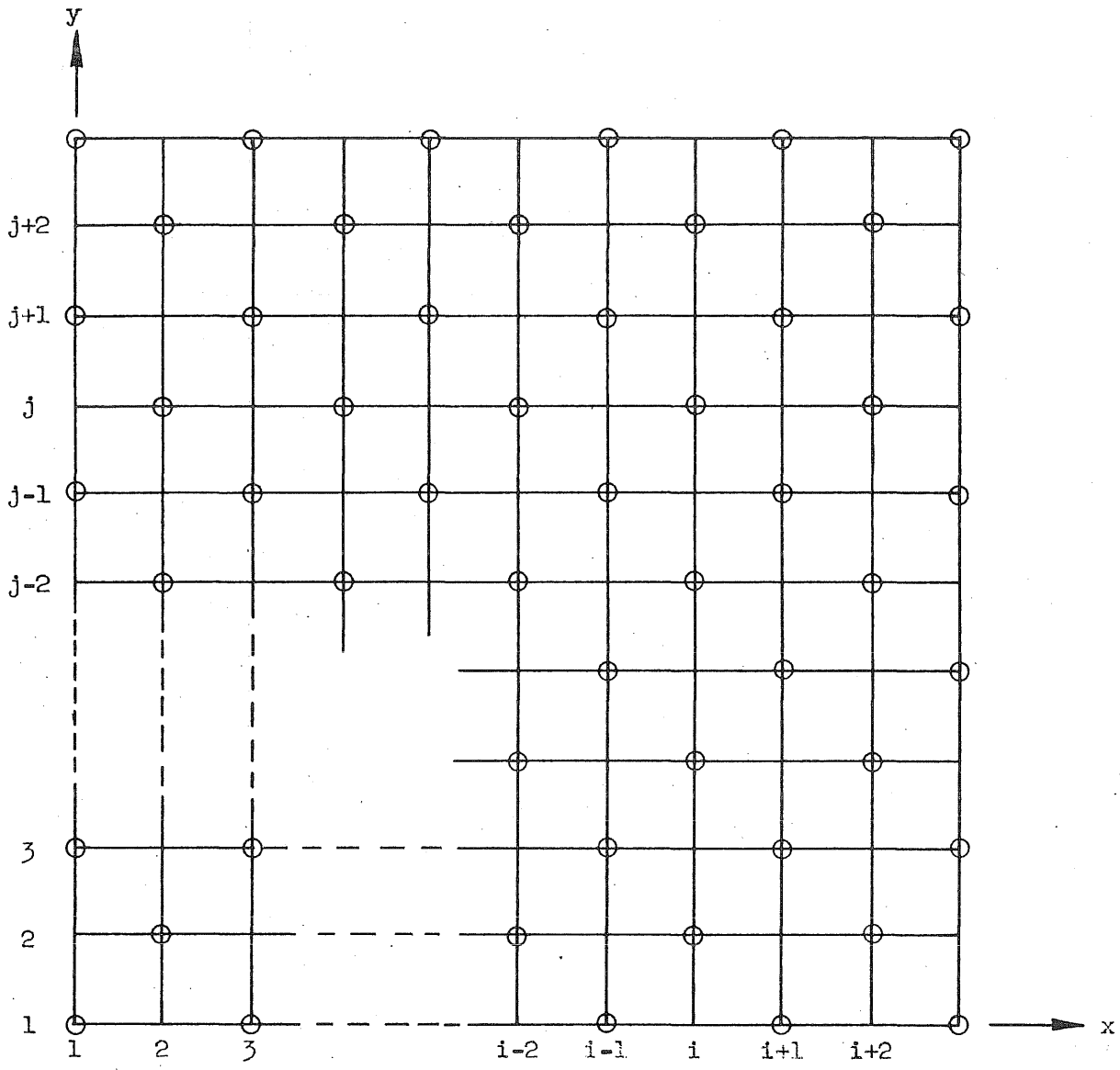

FIG. 5 GRID POINT IDENTIFICATION

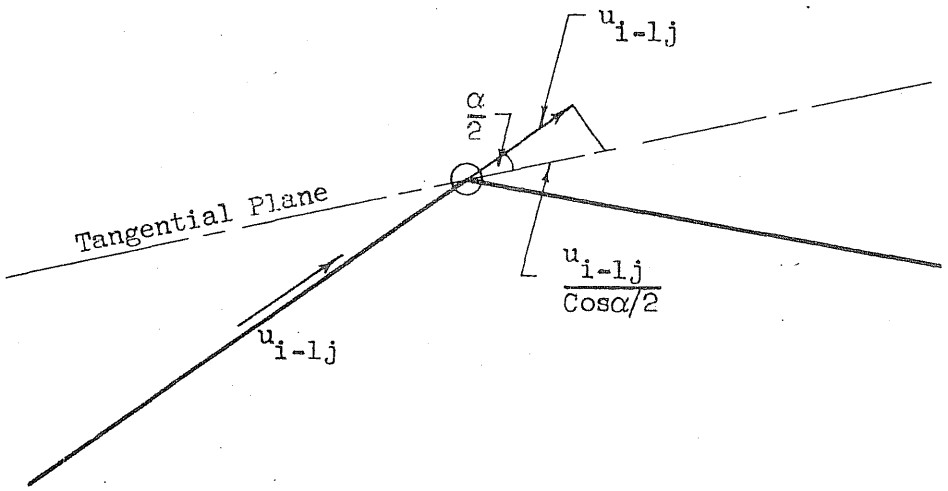

FIG. 6 TRANSFORMATION OF u DISPLACEMENT INTO TANGENTIAL PLANE

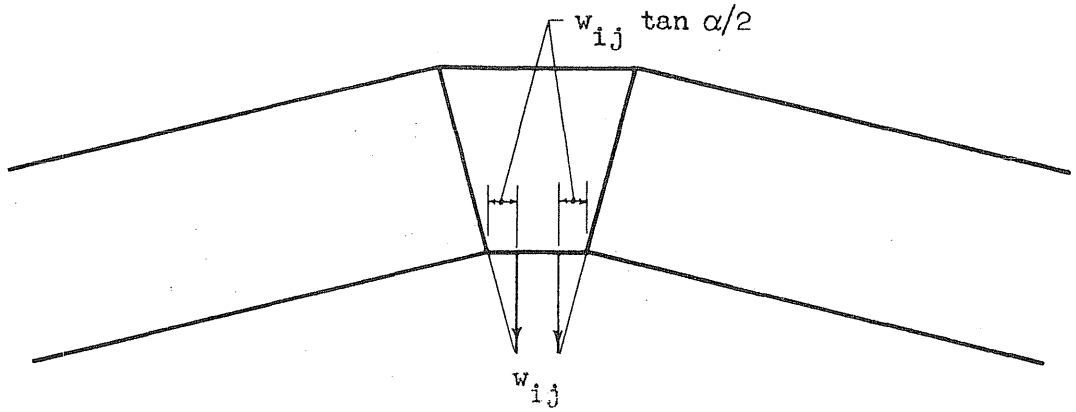

$$\sin \alpha/2 = \frac{L_{x/2}}{R_x} \qquad \tan \alpha/2 = \frac{L_x}{2R_x \cos\alpha/2}$$

FIG. 7 EFFECT OF w DISPLACEMENT ON EXTENSIONAL STRAIN

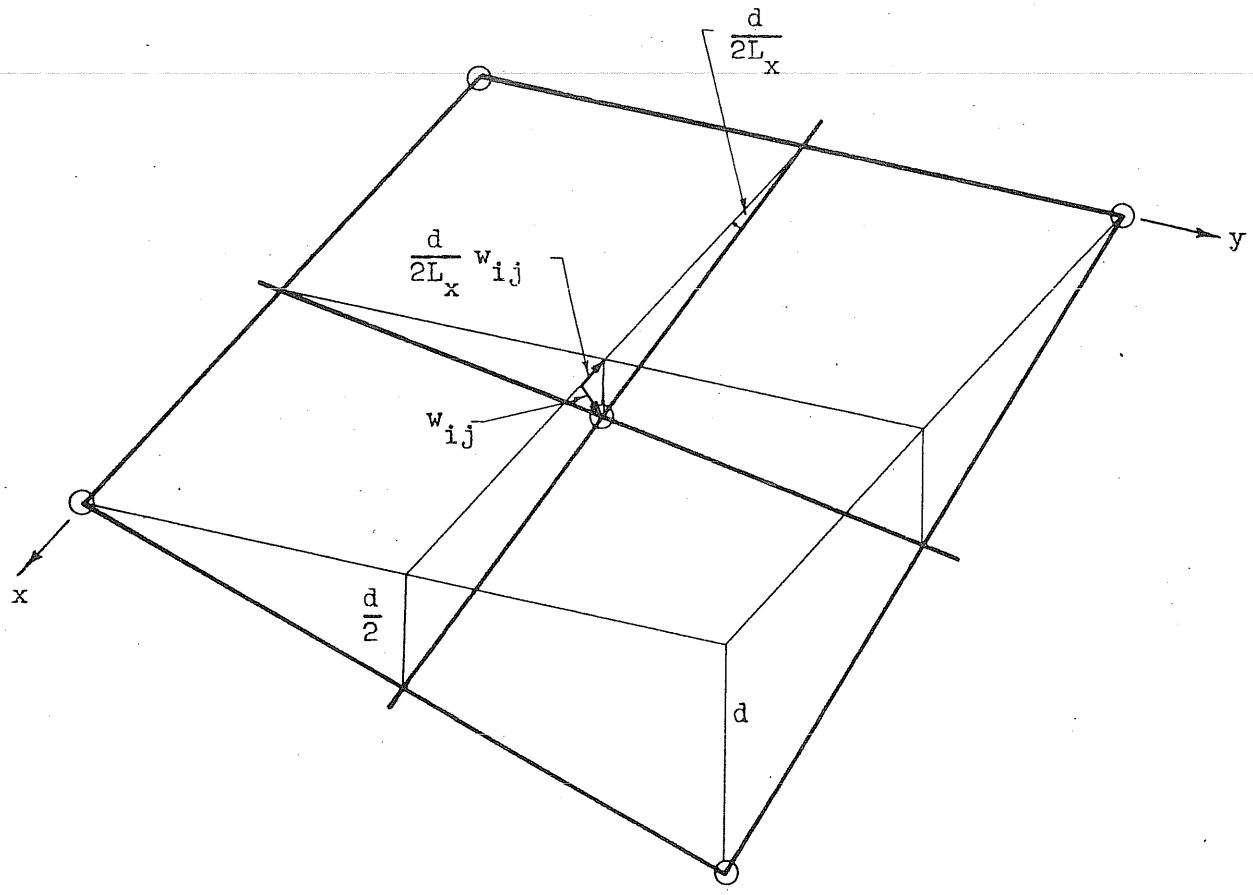

$$\epsilon^{w}_{xyij} = \frac{1}{L_{y/2}} \left(- \frac{d}{2L_x} w_{ij}\right) + \frac{1}{L_{x/2}} \left(- \frac{d}{2L_y} w_{ij}\right)$$

FIG. 8 EFFECT OF w DISPLACEMENT ON SHEAR STRAIN DUE TO THE TWIST OF THE ELEMENT

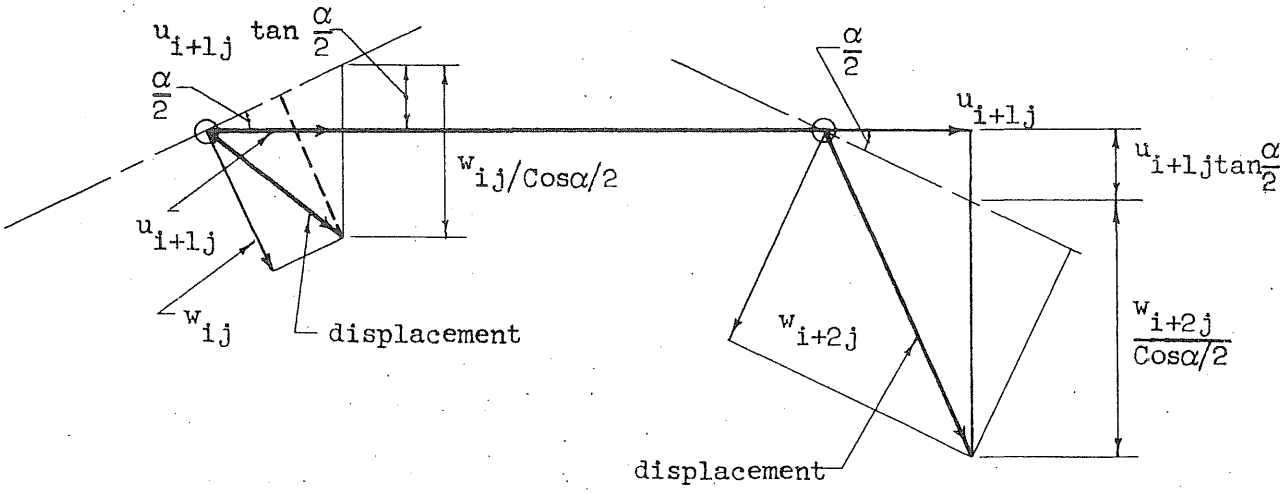

$$\theta_{xi+1j} = \frac{1}{L_x}\left[2u_{i+1j}\tan\alpha/2 + \frac{1}{\cos\alpha/2}\left(w_{i+2j}-w_{ij}\right)\right]$$

FIG. 9 ROTATION OF RIGID BAR ij,i+2j

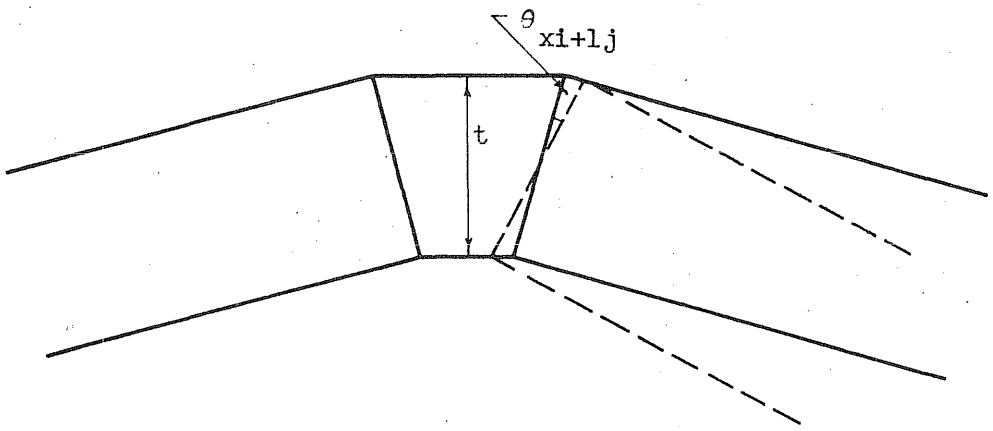

FIG. 10 EFFECT OF ROTATION OF RIGID BAR ON FLEXURAL STRAIN

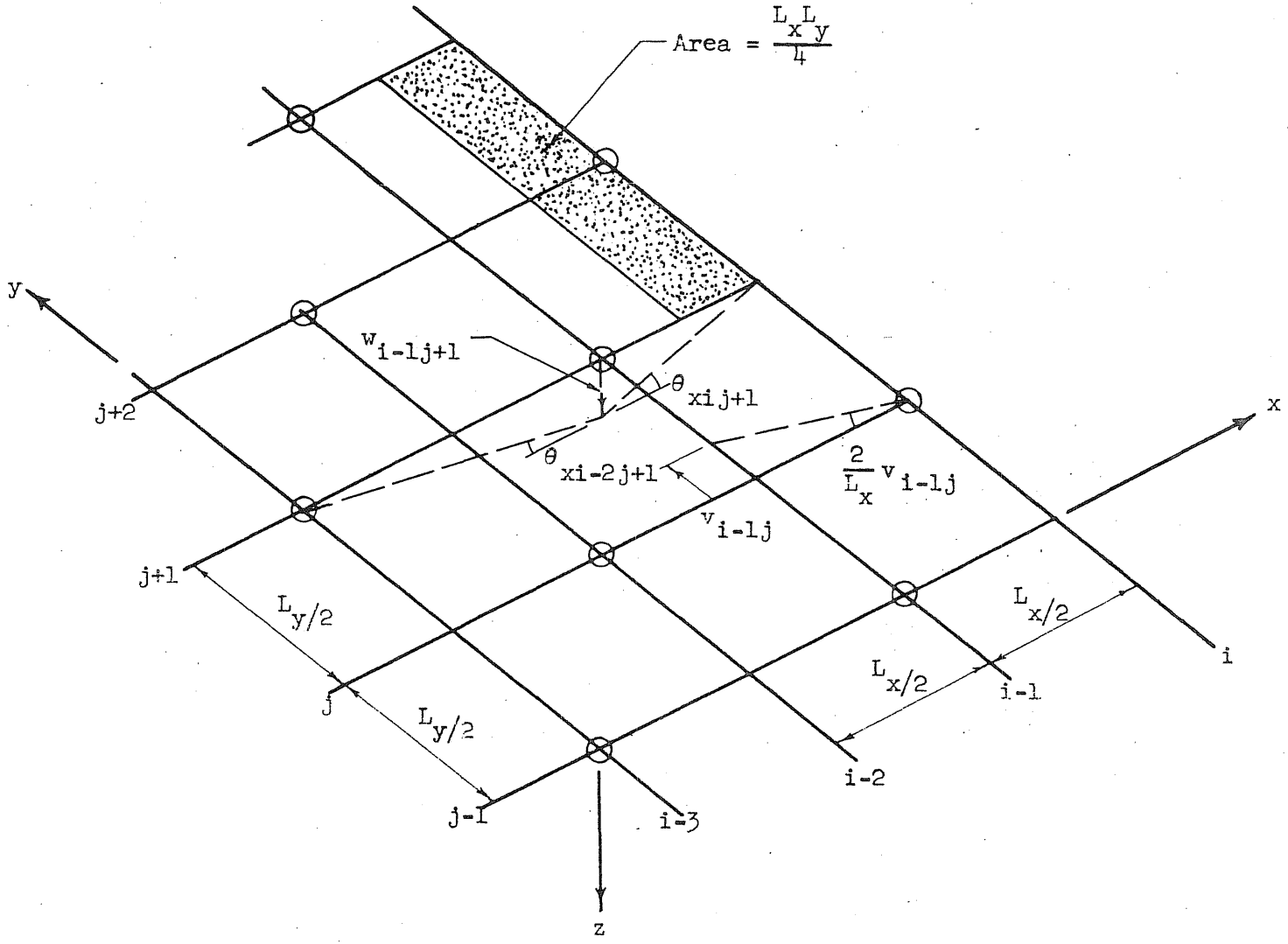

FIG. 11 SIMPLY SUPPORTED EDGE

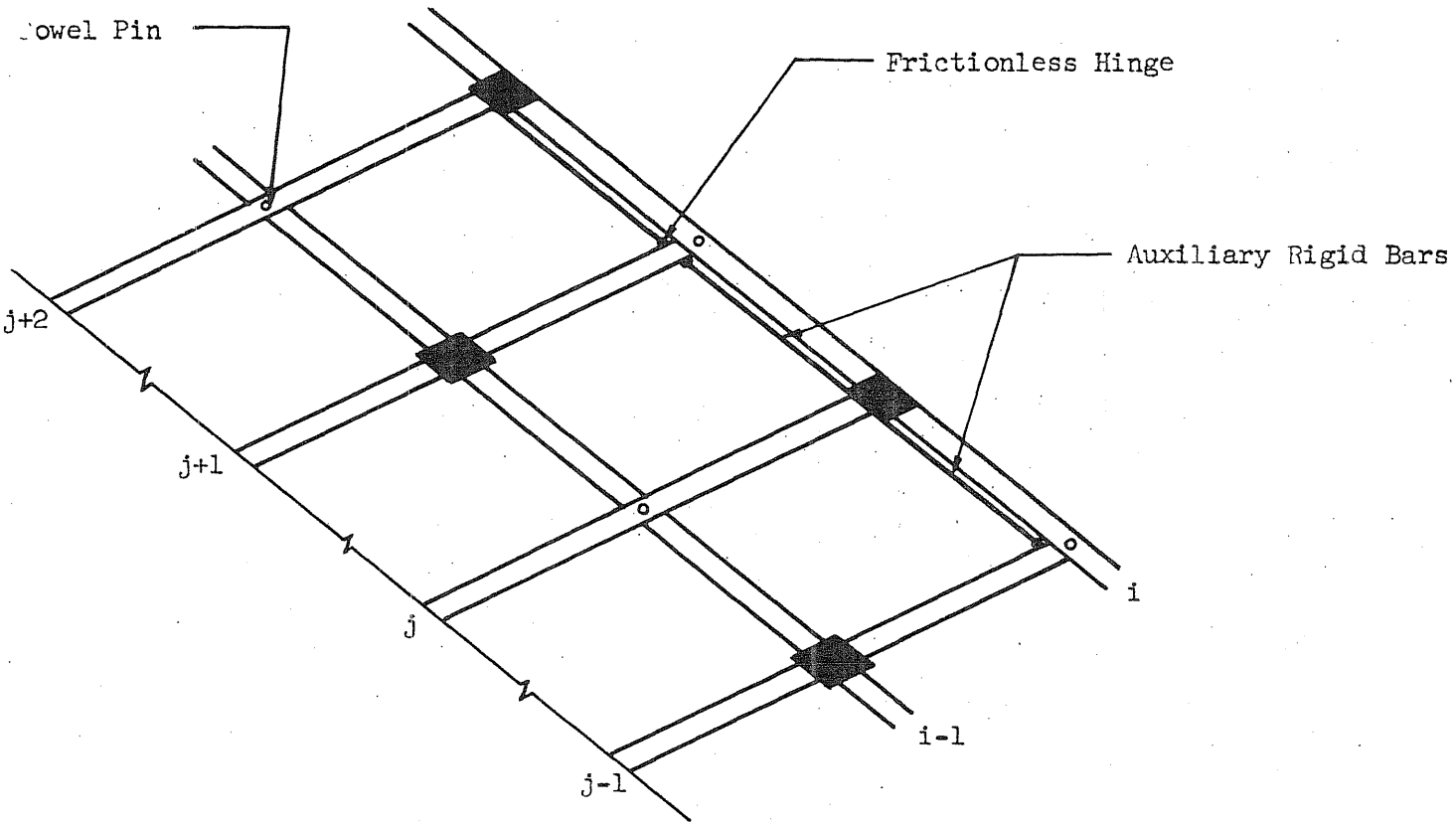

FIG. 12 LOCATION OF AUXILIARY RIGID BARS AT THE FREE EDGE

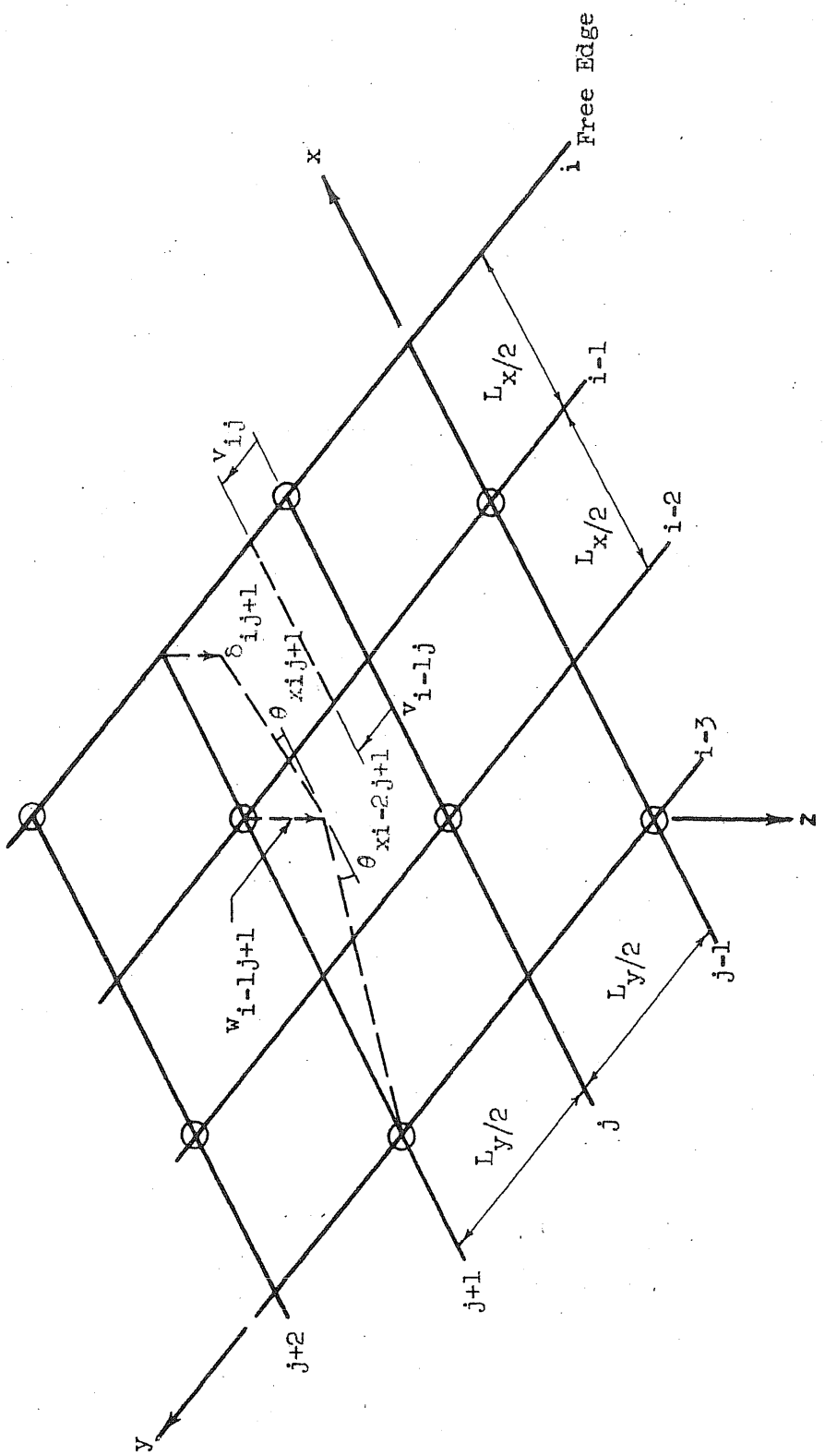

FIG. 13 FREE EDGE

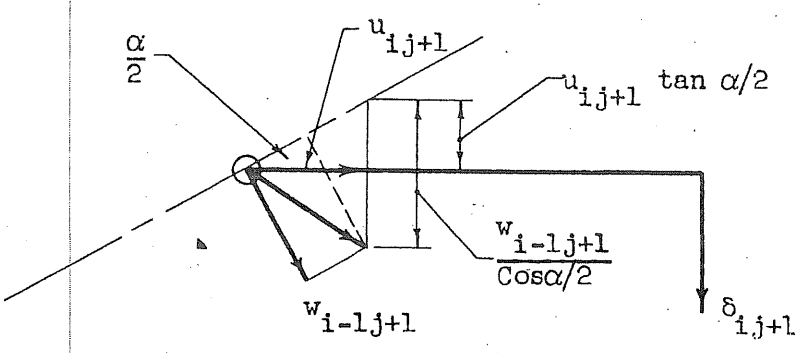

FIG. 14a ROTATION OF BAR i-1j+1,ij+1

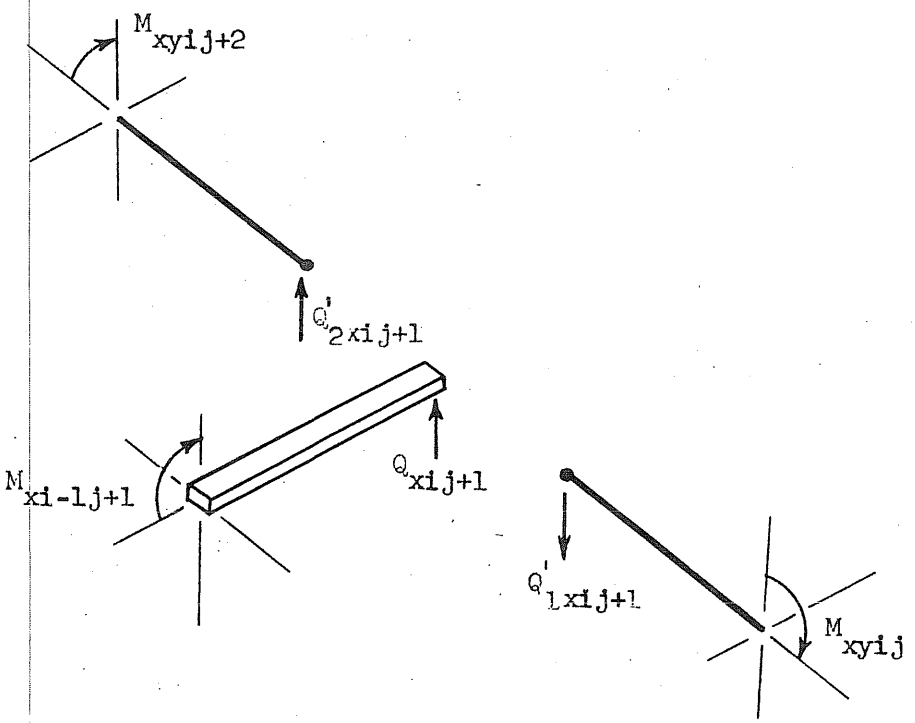

FIG. 14b EQUILIBRIUM AT FREE EDGE

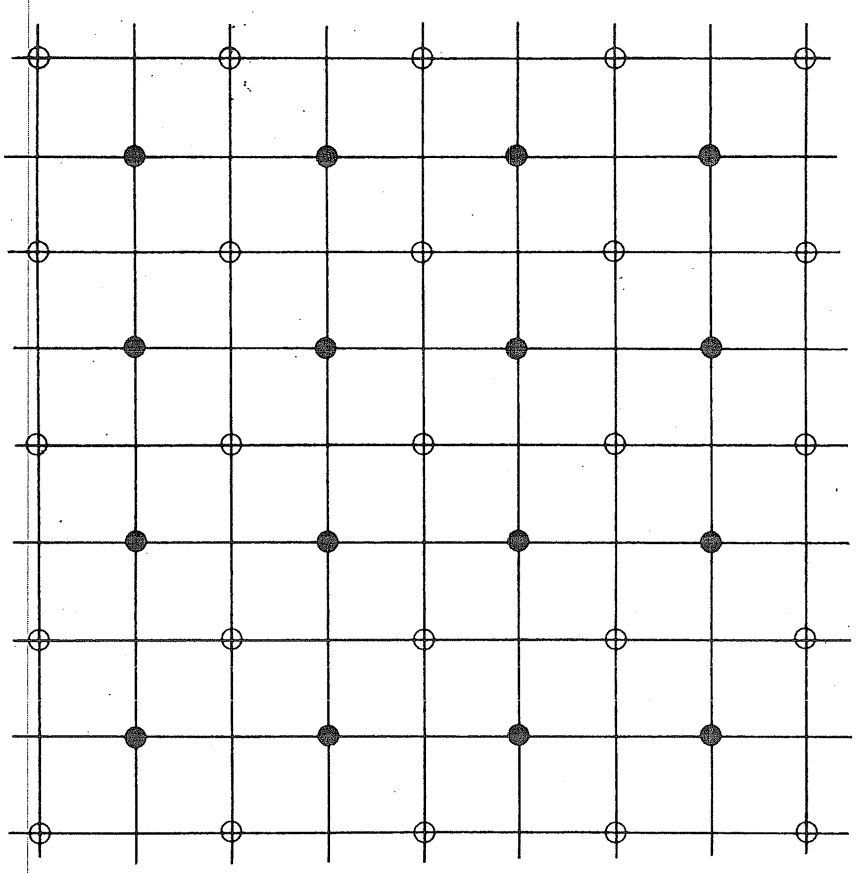

FIG. 15 SEPARATION OF THE TWO NETWORKS IN FLAT PLATES.

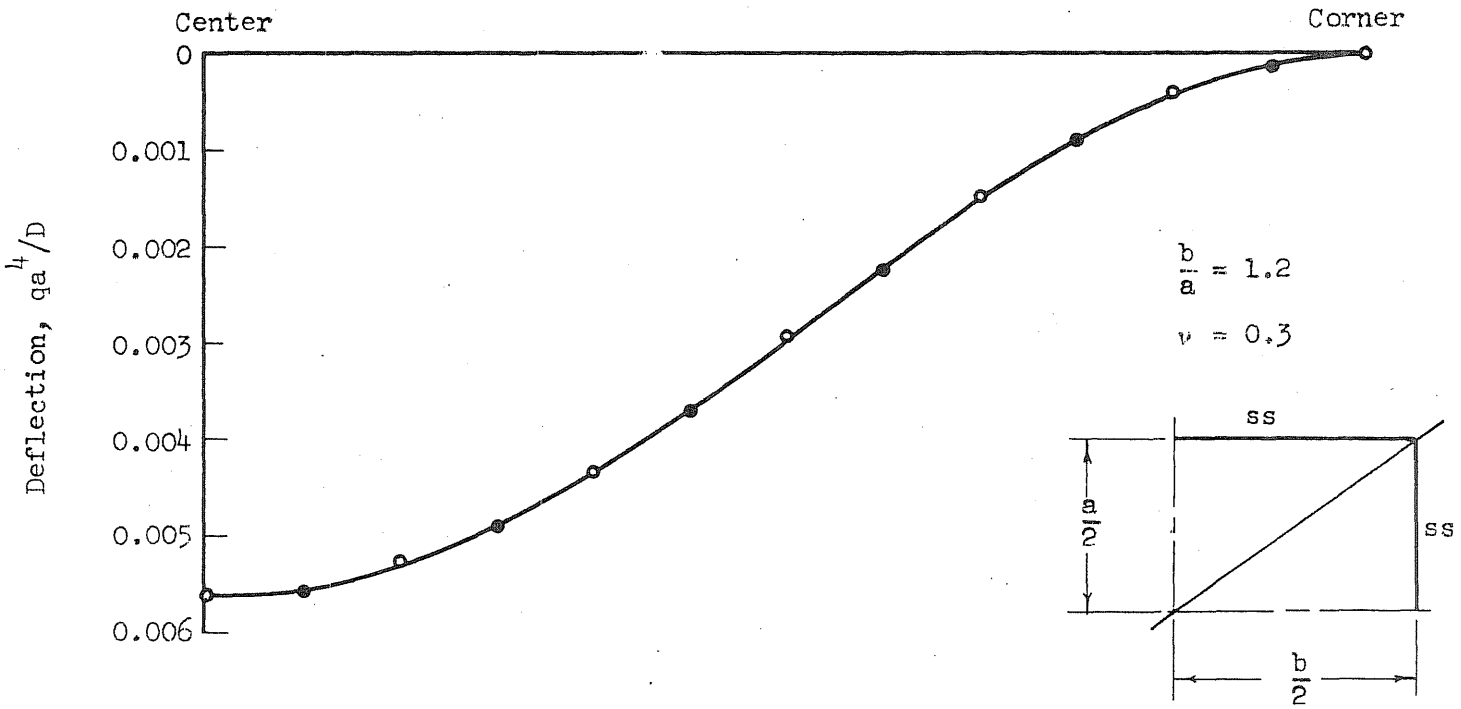

FIG. 16 DEFLECTIONS ALONG DIAGONAL OF A UNIFORMLY LOADED, SIMPLY SUPPORTED RECTANGULAR PLATE

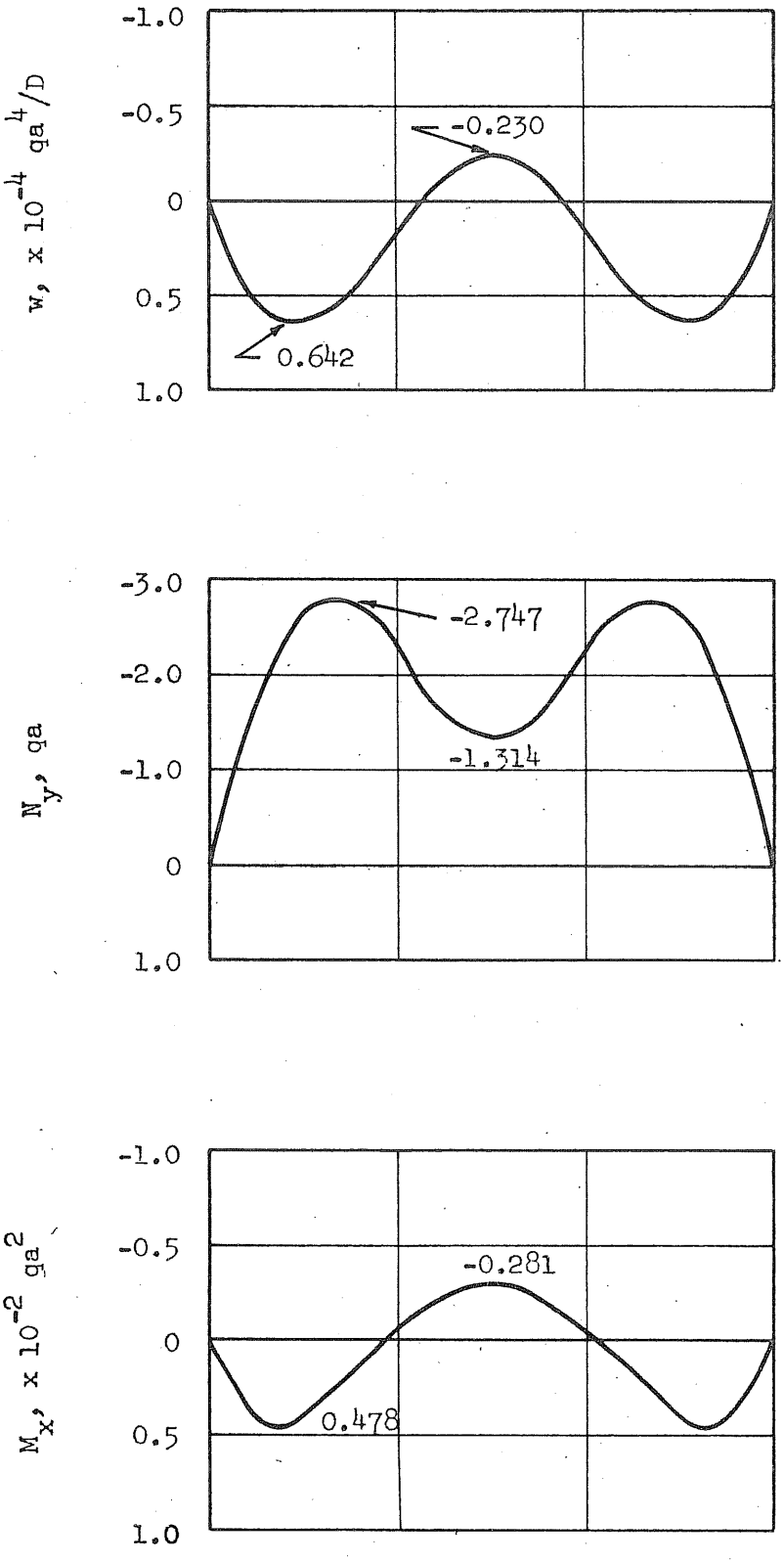

FIG. 17 THE DISPLACEMENTS w, THE FORCES N_y, AND THE BENDING MOMENTS M_x AT THE MIDSECTION OF A CYLINDRICAL SHELL, ALL EDGES SIMPLY SUPPORTED

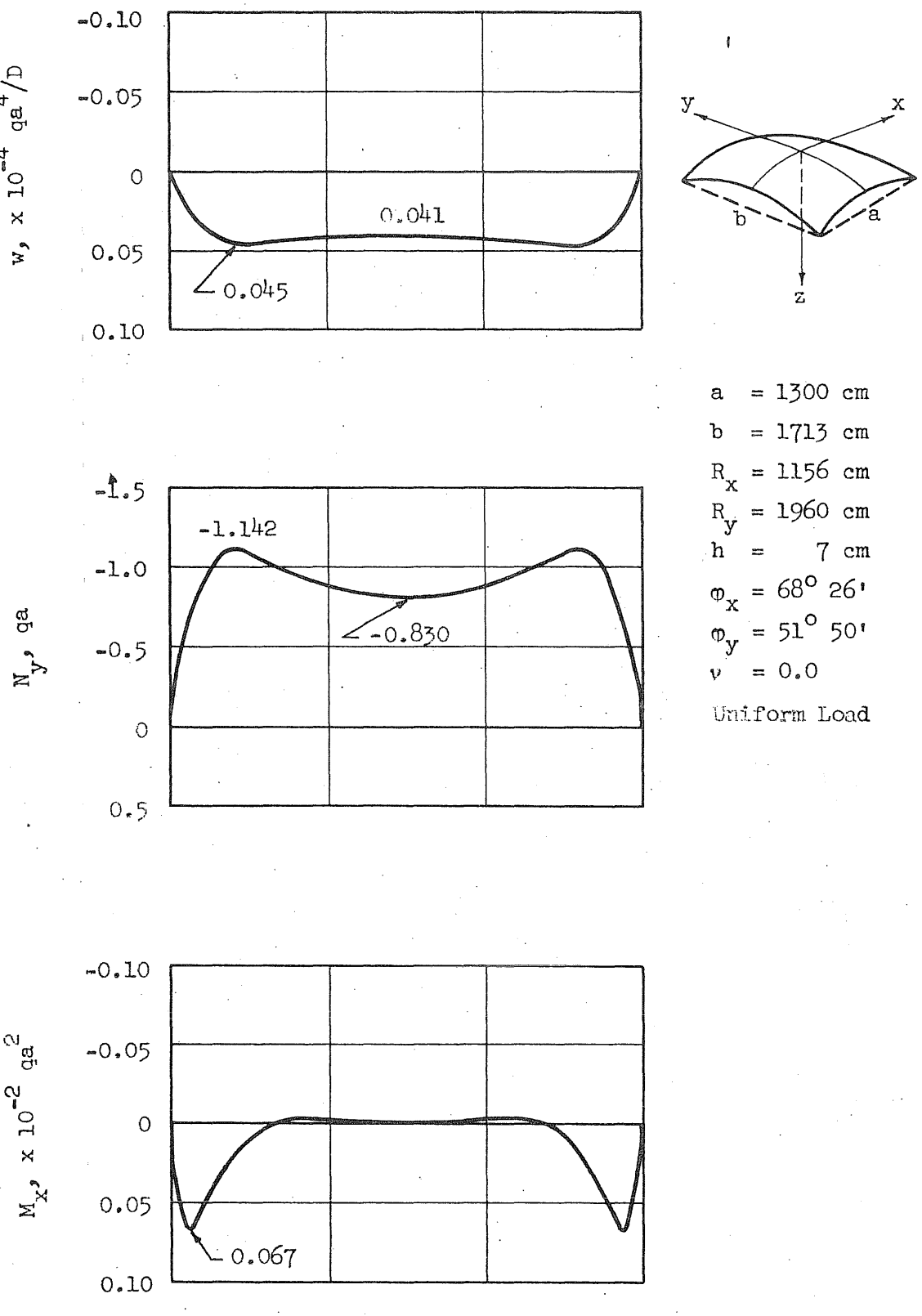

FIG. 18 THE DISPLACEMENTS w, THE FORCES N_y, AND THE BENDING MOMENTS M_x AT THE MIDSECTION OF AN ELLIPTIC PARABOLOID SHELL, ALL EDGES SIMPLY SUPPORTED

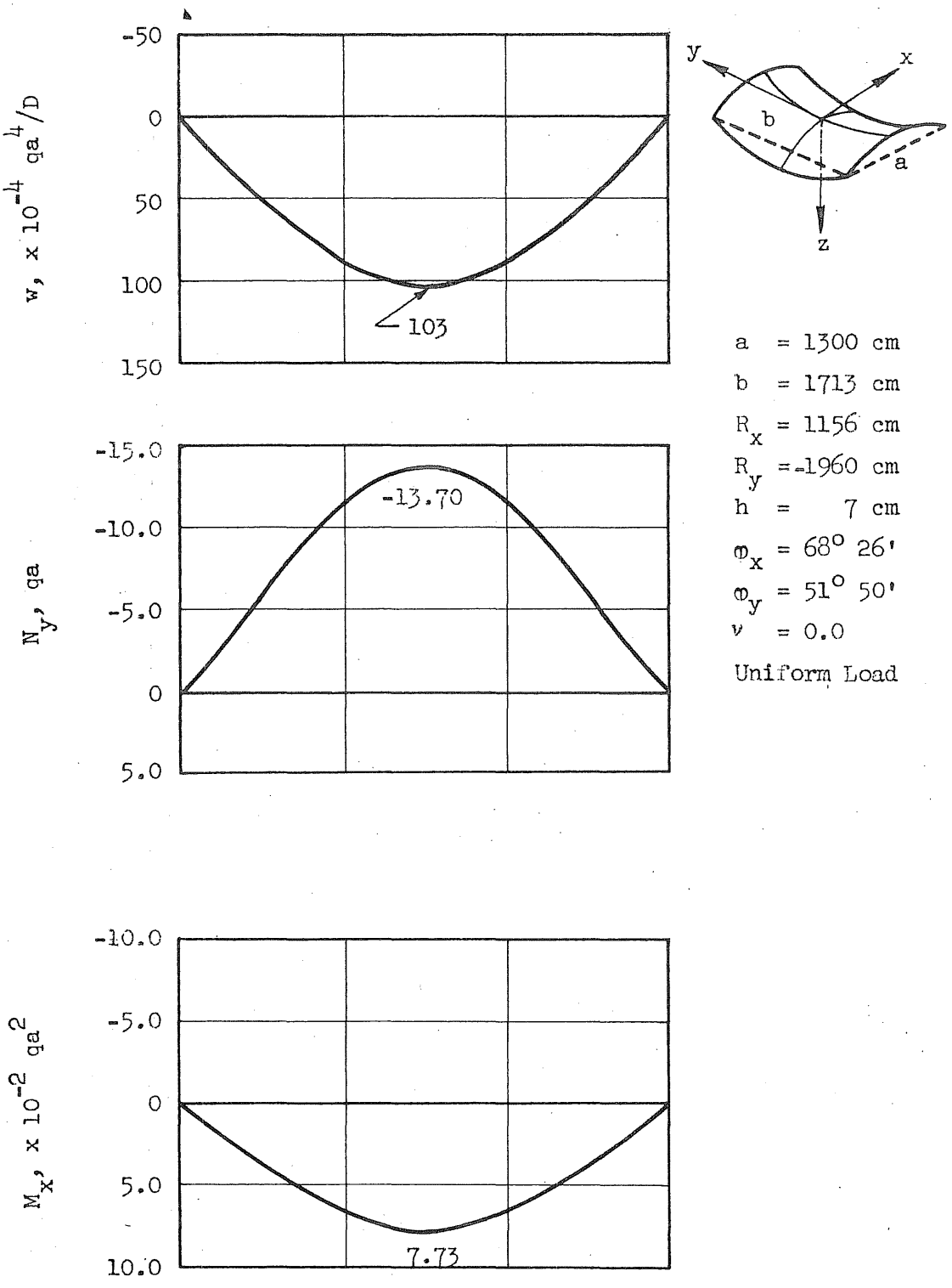

FIG. 19 THE DISPLACEMENTS w, THE FORCES N_y, AND THE BENDING MOMENTS M_x AT THE MIDSECTION OF A HYPERBOLIC PARABOLOID SHELL, ALL EDGES SIMPLY SUPPORTED

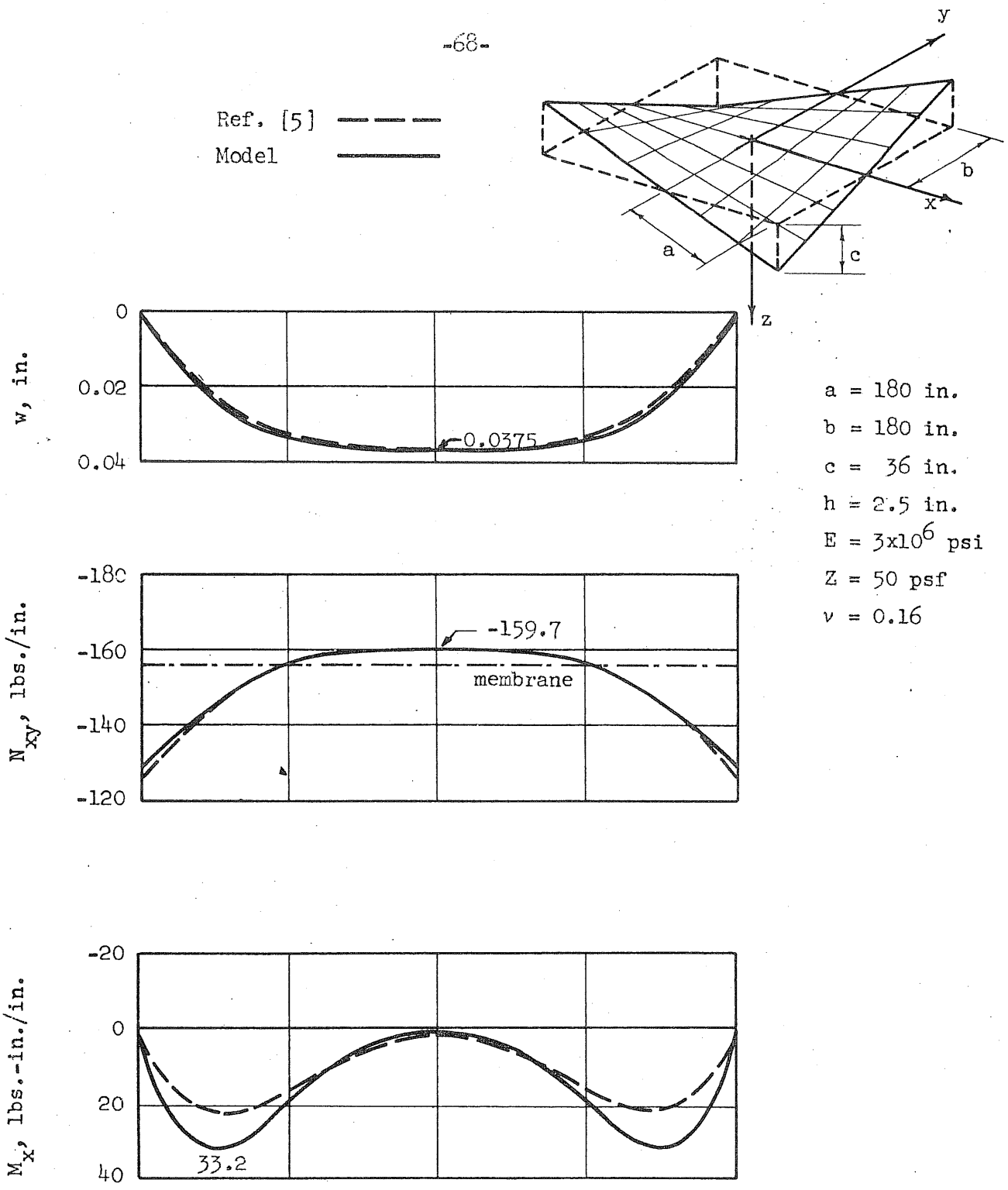

FIG. 20 THE DISPLACEMENTS w, THE FORCES N_{xy}, AND THE BENDING MOMENTS M_x AT THE MIDSECTION OF A SIMPLY SUPPORTED HYPERBOLIC PARABOLOID SHELL BOUNDED BY CHARACTERISTICS

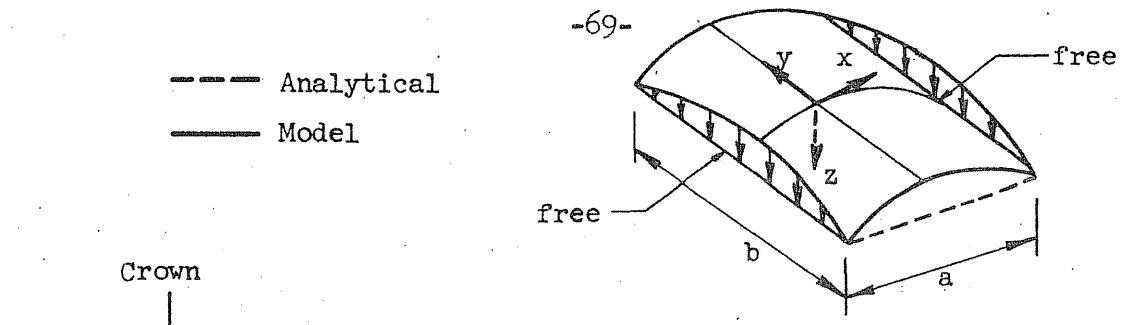

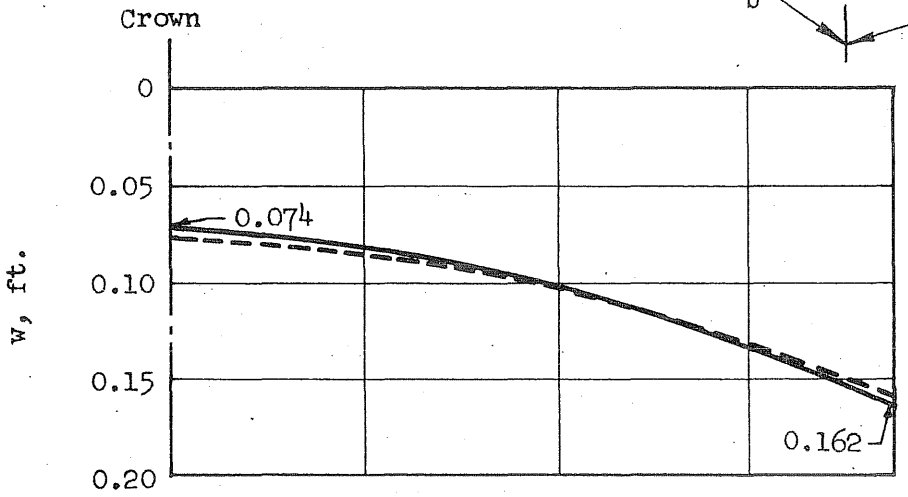

a = 25.88 ft.
b = 50.00 ft.
R_x = 50.00 ft.
h = 0.50 ft.
φ_x = 30° 00'
ν = 0.15
E = 4.32×10^5 ksf
Z = $\cos \frac{\pi}{b} y$

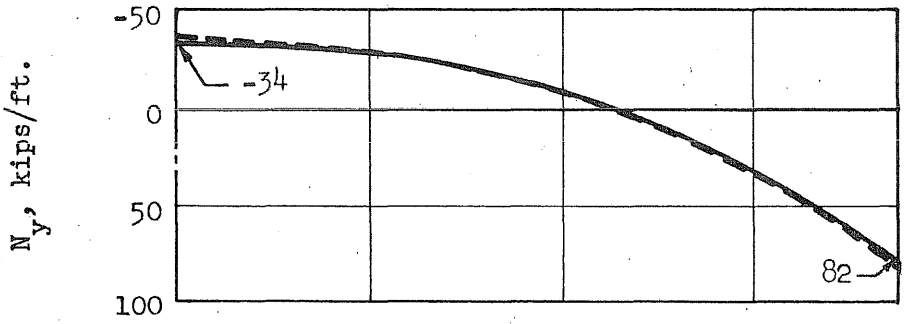

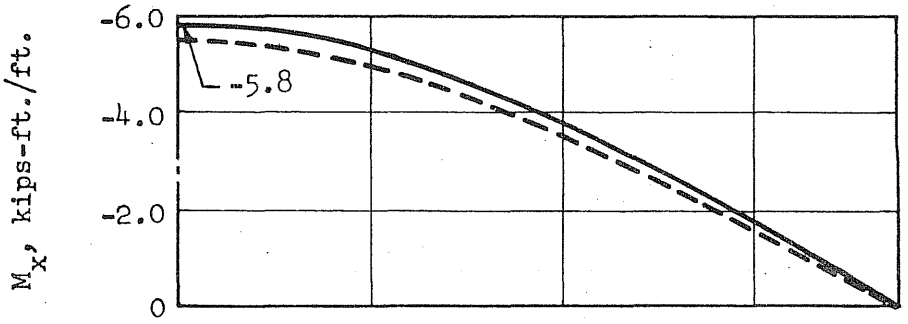

FIG. 21 THE DISPLACEMENTS w, THE FORCES N_y, AND THE BENDING MOMENTS M_x AT THE MIDSECTION OF A CYLINDRICAL SHELL, TWO EDGES SIMPLY SUPPORTED AND THE REMAINING TWO EDGES FREE

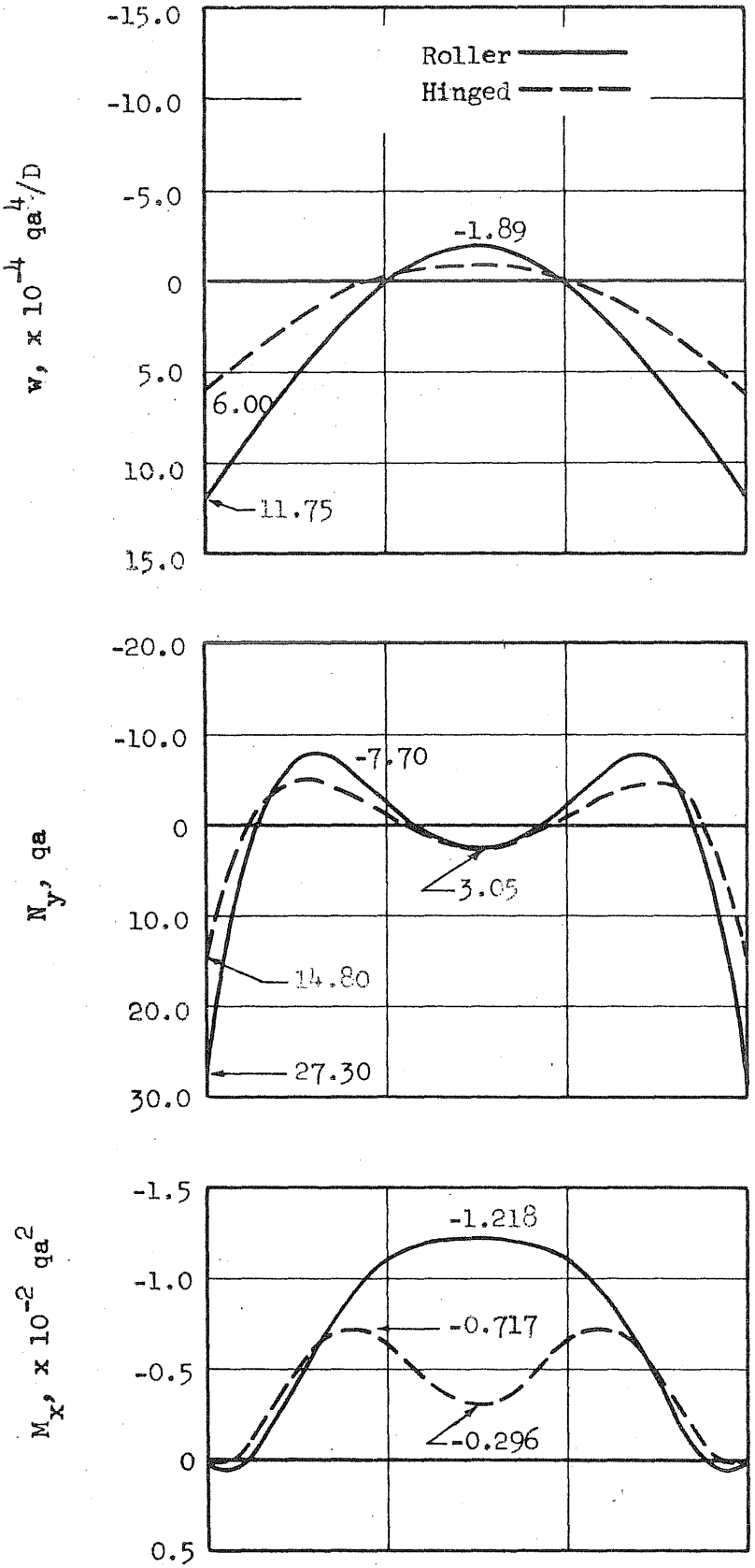

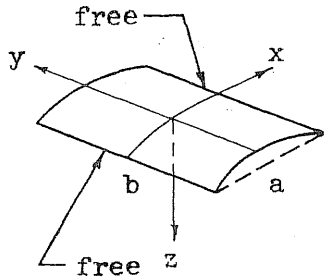

a = 1300 cm
b = 1800 cm
R_x = 1156 cm
h = 7 cm
φ_x = 68° 26'
ν = 0.0
Z = q Cos $\frac{\pi}{b}$ y

FIG. 22 THE DISPLACEMENTS w, THE FORCES N_y, AND THE BENDING MOMENTS M_x AT THE MIDSECTION OF A CYLINDRICAL SHELL, TWO EDGES SIMPLY SUPPORTED AND THE REMAINING TWO EDGES FREE

Roller ———

Hinged — — —

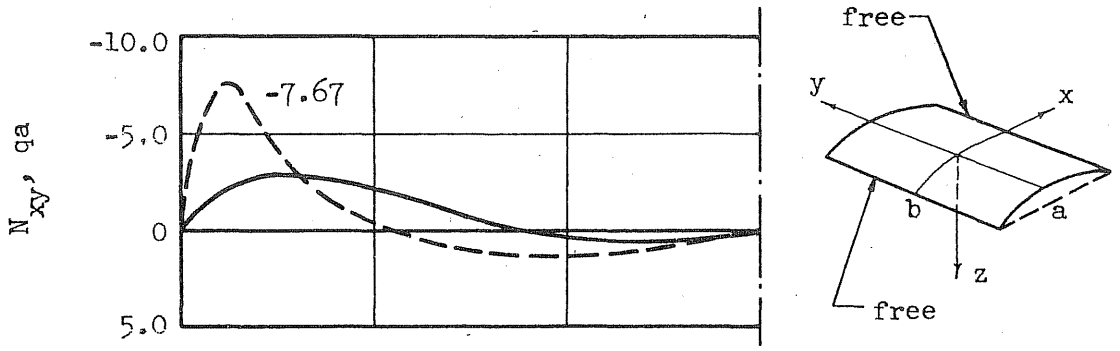

a = 1300 cm

b = 1800 cm

R_x = 1156 cm

h = 7 cm

$\Phi_x = 68^\circ\ 26'$

ν = 0.0

$Z = q \cos \frac{\pi}{b} y$

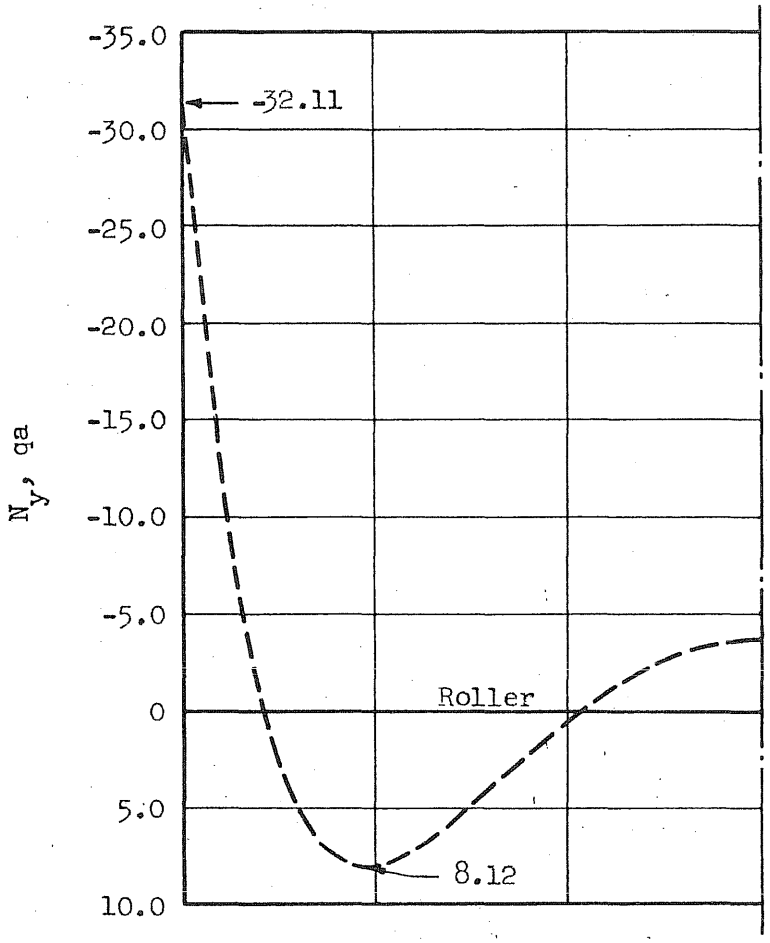

FIG. 23 THE FORCES N_{xy} AND N_y AT THE SUPPORTED EDGE OF A CYLINDRICAL SHELL, TWO EDGES SIMPLY SUPPORTED AND THE REMAINING TWO EDGES FREE

12 x 6 ———

6 x 6 – – – –

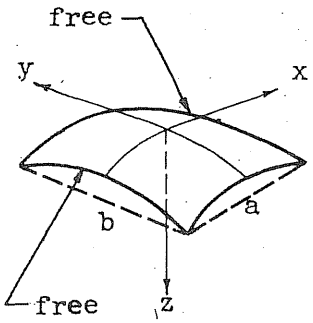

a = 1300 cm

b = 1713 cm

R_x = 1156 cm

R_y = 1960 cm

h = 7 cm

φ_x = 68° 26'

φ_y = 51° 50'

ν = 0.0

Z = q Cos $\frac{\pi}{b}$ y

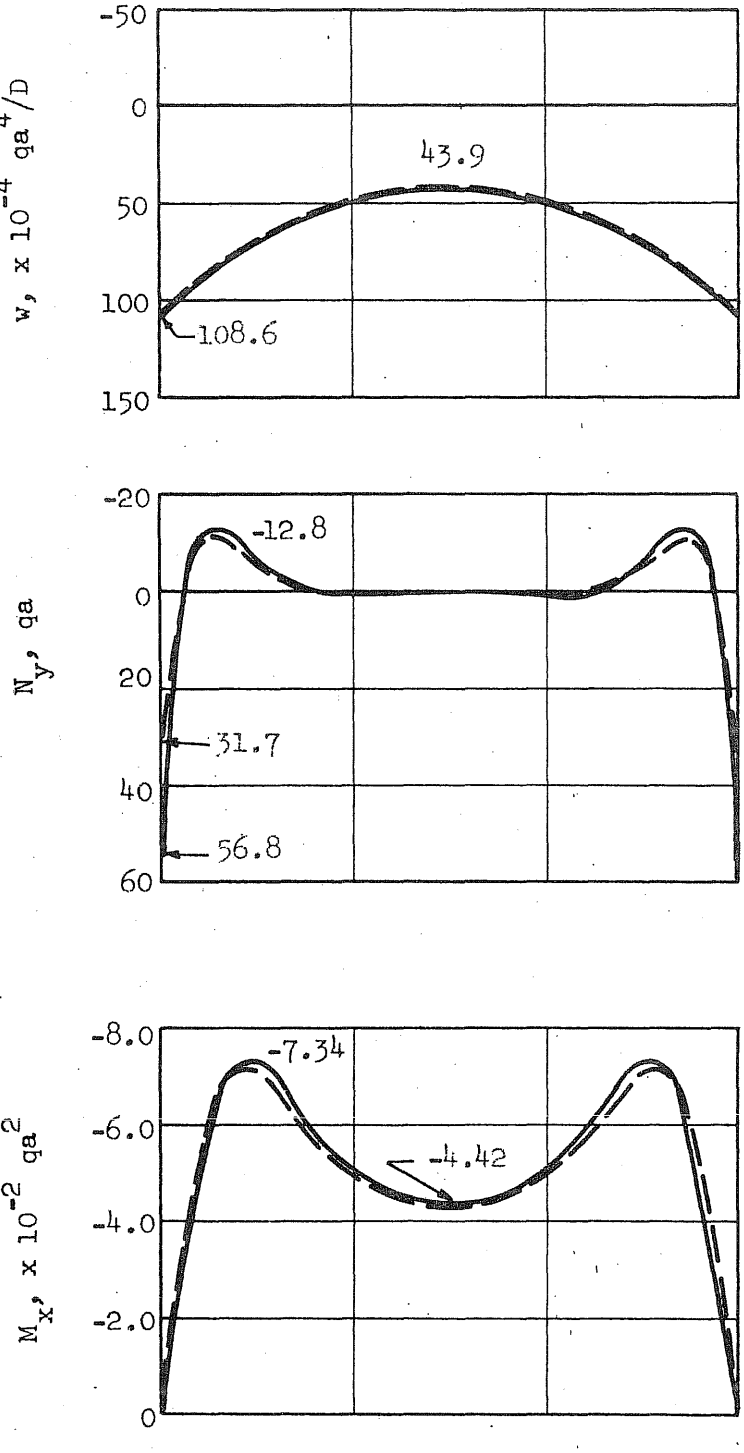

FIG. 24 THE DISPLACEMENTS w, THE FORCES N_y, AND THE BENDING MOMENTS M_x AT THE MIDSECTION OF AN ELLIPTIC PARABOLOID SHELL, TWO EDGES SIMPLY SUPPORTED AND THE REMAINING TWO EDGES FREE

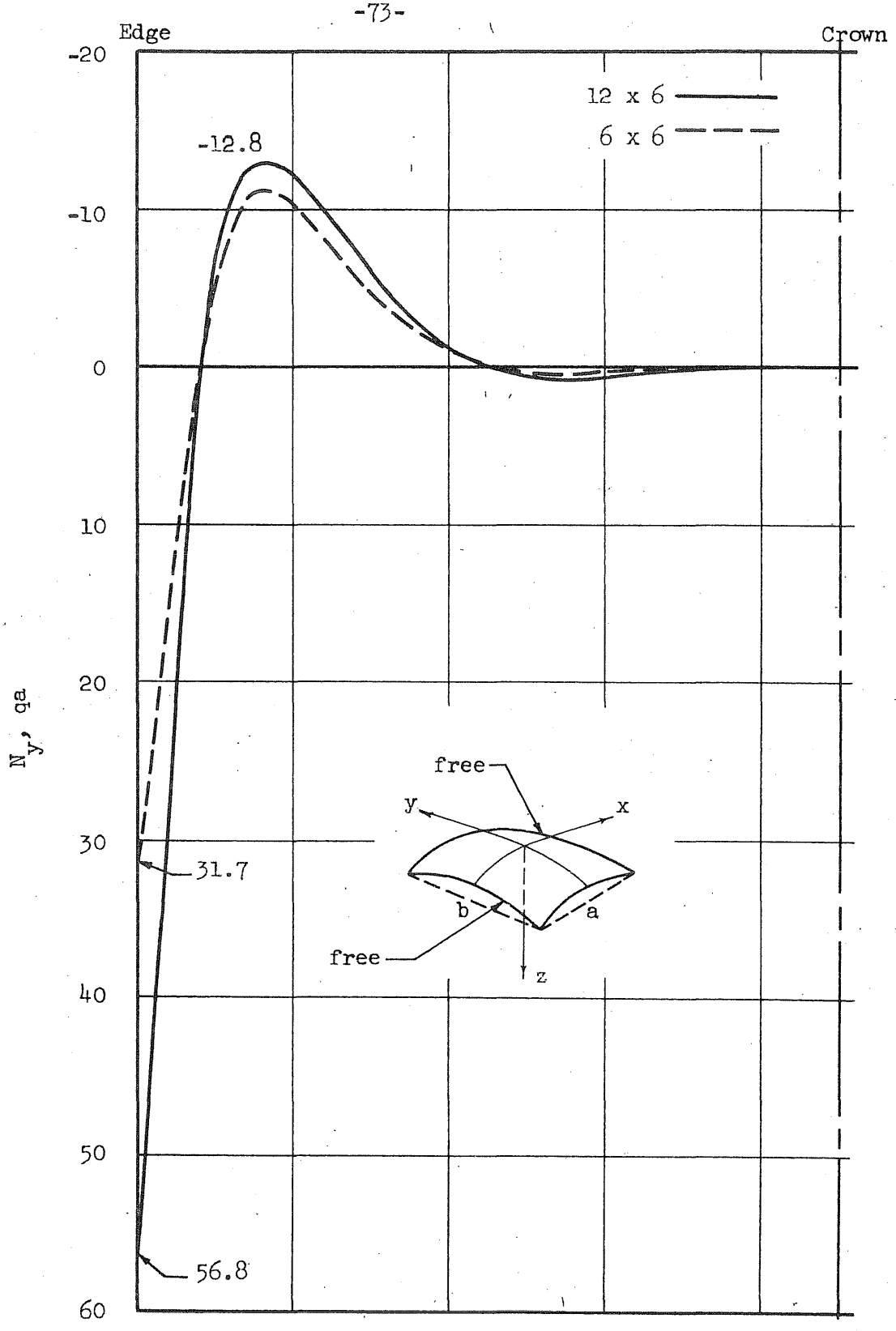

FIG. 25 THE FORCES N_y AT THE MIDSECTION OF AN ELLIPTIC PARABOLOID SHELL, TWO EDGES SIMPLY SUPPORTED AND THE REMAINING TWO EDGES FREE

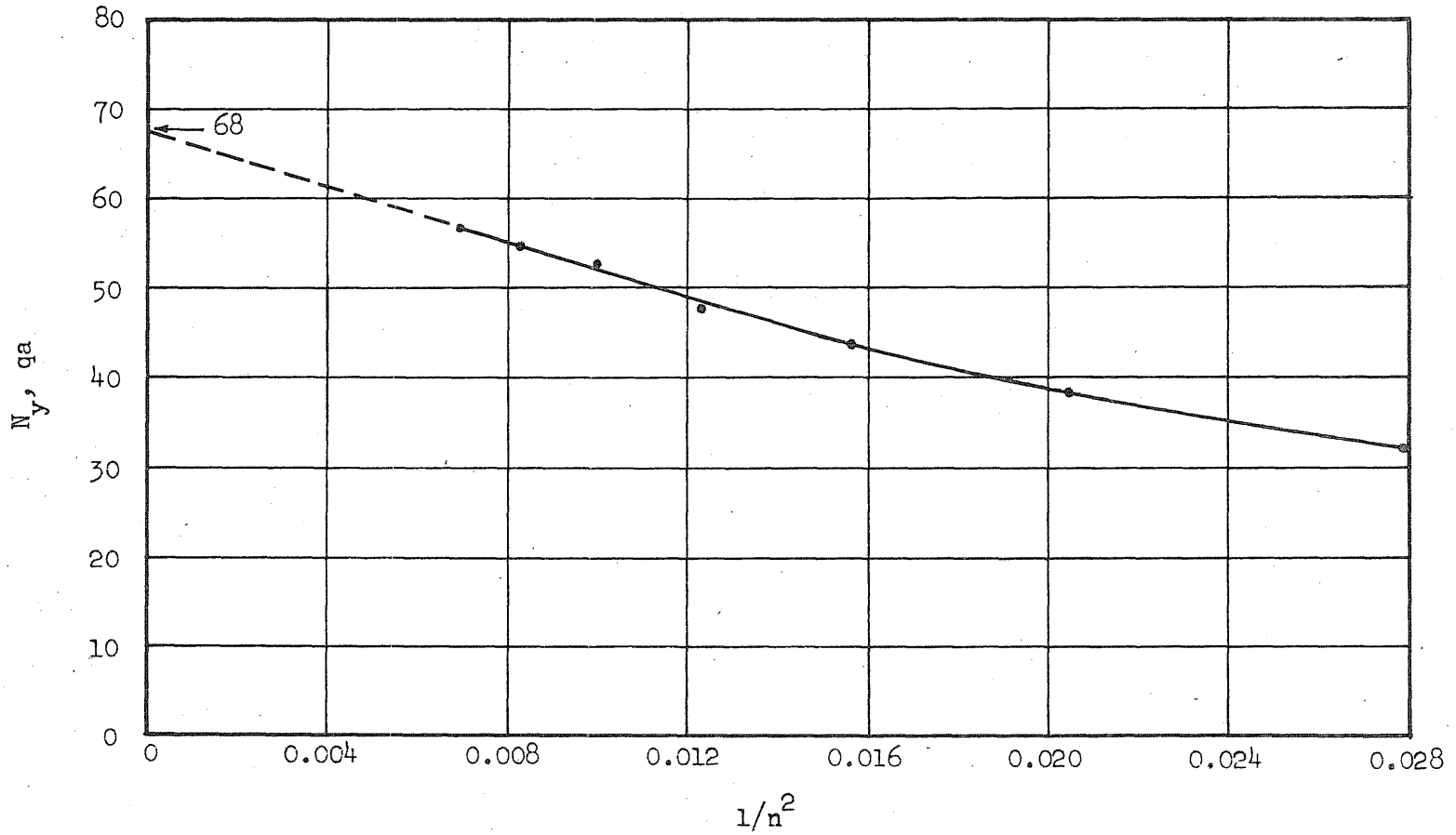

FIG. 26 THE PLOT OF THE FORCES N_y AT FREE EDGE VS INVERSE OF THE SQUARE OF NUMBER OF SPACINGS FOR AN ELLIPTIC PARABOLOID SHELL, TWO EDGES SIMPLY SUPPORTED AND THE REMAINING TWO EDGES FREE

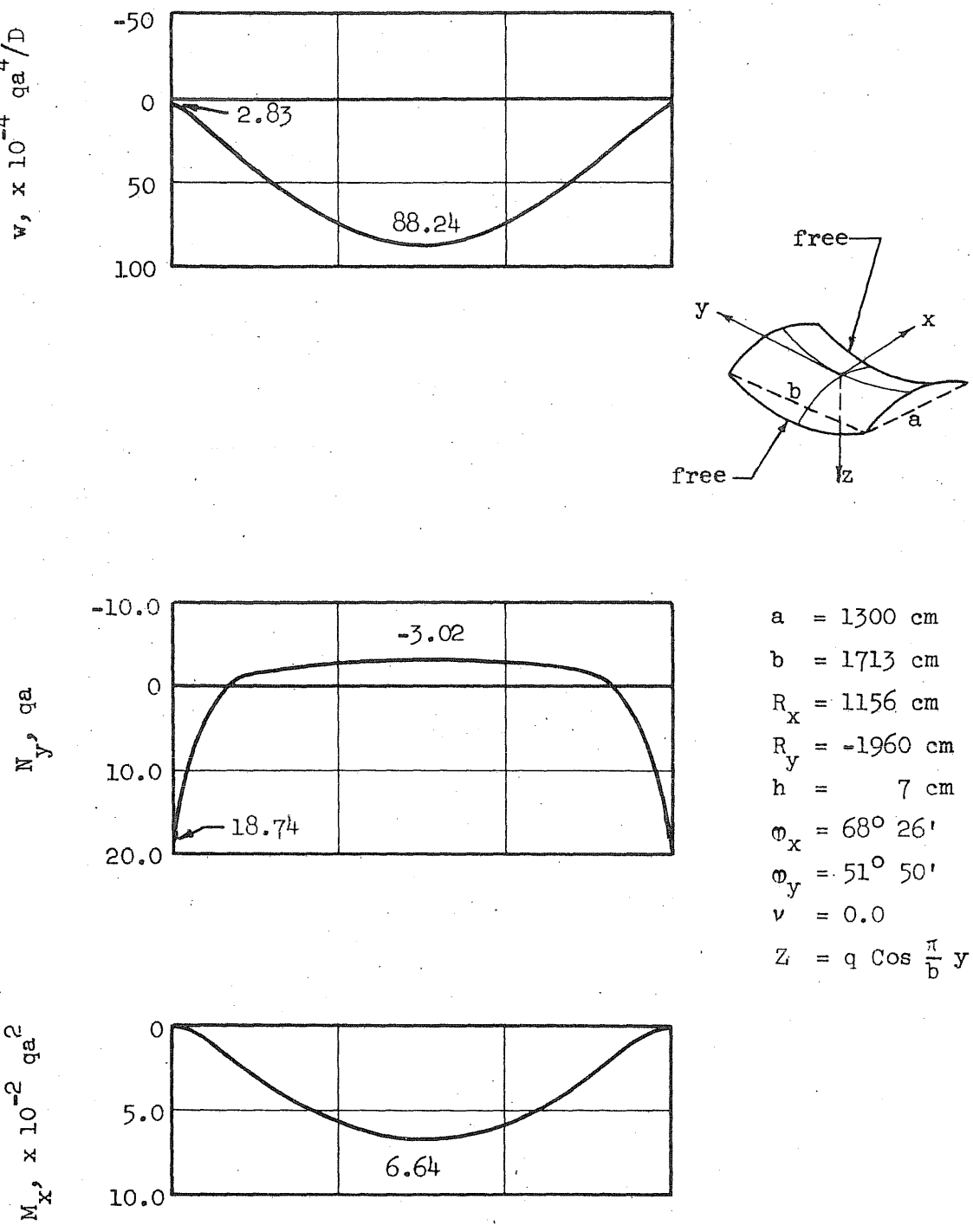

$a = 1300$ cm

$b = 1713$ cm

$R_x = 1156$ cm

$R_y = -1960$ cm

$h = 7$ cm

$\varphi_x = 68^\circ 26'$

$\varphi_y = 51^\circ 50'$

$\nu = 0.0$

$Z = q \cos \frac{\pi}{b} y$

FIG. 27 THE DISPLACEMENTS w, THE FORCES N_y, AND THE BENDING MOMENT M_x AT THE MIDSECTION OF A HYPERBOLIC PARABOLOID SHELL, TWO EDGES SIMPLY SUPPORTED AND THE REMAINING TWO EDGES FREE

APPENDIX A

EQUILIBRIUM EQUATIONS

Although the equilibrium equations of the model are generated within a digital computer, the equilibrium equations of typical interior points are presented here for reference.

The equilibrium equation in the x direction at point i+1j is

$$\frac{L_x L_y}{2}\left[\left(\frac{1}{\cos^2 \alpha/2} + \frac{t^2}{4R_x^2 \cos^2 \alpha/2}\right)\frac{1}{L_x^2}\left(u_{i+3j} - 2u_{i+1j} + u_{i-1j}\right)\right.$$

$$+ \frac{1-\nu}{2}\left(1 + \frac{t^2}{4R_x^2 \cos^2 \alpha/2}\right)\frac{1}{L_y^2}\left(u_{i+1j+2} - 2u_{i+1j} + u_{i+1j-2}\right)$$

$$+ \left(\frac{1-\nu}{2} + \frac{\nu}{\cos \alpha/2 \cos \beta/2} + \frac{1+\nu}{2}\,\frac{t^2}{4R_x R_y \cos \alpha/2 \cos \beta/2}\right)\frac{1}{L_x L_y}\left(v_{i+2j+1}\right.$$

$$\left. - v_{i+2j-1} - v_{ij+1} + v_{ij-1}\right) - \left(\frac{1}{R_x \cos^2 \alpha/2} + \frac{\nu}{R_y \cos \alpha/2 \cos \beta/2}\right)\frac{1}{L_x}\left(w_{i+2j} - w_{ij}\right)$$

$$- \frac{1-\nu}{L_x L_y}\frac{d}{L_y}\left(w_{i+1j+1} - w_{i+1j-1}\right) + \frac{t^2}{4R_x \cos^2 \alpha/2}\frac{1}{L_x^3}\left(w_{i+4j} - 3w_{i+2j} + 3w_{ij} - w_{i-2j}\right)$$

$$+ \frac{t^2}{4R_x \cos \alpha/2}\left(\frac{1-\nu}{2}\,\frac{1}{\cos \alpha/2} + \frac{1+\nu}{2}\,\frac{1}{\cos \beta/2}\right)\frac{1}{L_x L_y^2}\left(w_{i+2j+2} - 2w_{i+2j} + w_{i+2j-2}\right.$$

$$\left.\left. - w_{ij+2} + 2w_{ij} - w_{ij-2}\right)\right] + \frac{1-\nu^2}{Eh}\,\bar{X} = 0 \qquad \text{(A-1)}$$

The equilibrium equation in the y direction at point ij+1 is

$$\frac{L_x L_y}{2}\left[\left(\frac{1}{\cos^2\beta/2}+\frac{t^2}{4R_y^2\cos^2\beta/2}\right)\frac{1}{L_y^2}\left(v_{ij+3}-2v_{ij+1}+v_{ij-1}\right)\right.$$

$$+\frac{1-\nu}{2}\left(1+\frac{t^2}{4R_y^2\cos^2\beta/2}\right)\frac{1}{L_x^2}\left(v_{i+2j+1}-2v_{ij+1}+v_{i-2j+1}\right)$$

$$+\left(\frac{1-\nu}{2}+\frac{\nu}{\cos\alpha/2\cos\beta/2}+\frac{1+\nu}{2}\frac{t^2}{4R_xR_y\cos\alpha/2\cos\beta/2}\right)\frac{1}{L_xL_y}\left(u_{i+1j+2}-u_{i-1j+2}\right.$$

$$\left.-u_{i+1j}+u_{i-1j}\right)-\left(\frac{1}{R_y\cos^2\beta/2}+\frac{\nu}{R_x\cos\alpha/2\cos\beta/2}\right)\frac{1}{L_y}\left(w_{ij+2}-w_{ij}\right)$$

$$-\frac{1-\nu}{L_xL_y}\frac{d}{L_x}\left(w_{i+1j+1}-w_{i-1j+1}\right)+\frac{t^2}{4R_y\cos^2\beta/2}\frac{1}{L_y^3}\left(w_{ij+4}-3w_{ij+2}+3w_{ij}\right.$$

$$\left.-w_{ij-2}\right)+\frac{t^2}{4R_y\cos\beta/2}\left(\frac{1-\nu}{2}\frac{1}{\cos\beta/2}+\frac{1+\nu}{2}\frac{1}{\cos\alpha/2}\right)\frac{1}{L_x^2L_y}\left(w_{i+2j+2}-2w_{ij+2}\right.$$

$$\left.\left.+w_{i-2j+2}-w_{i+2j}+2w_{ij}-w_{i-2j}\right)\right]+\frac{1-\nu^2}{Eh}\bar{Y}=0 \qquad \text{(A-2)}$$

The equilibrium equation in the z direction at point ij is

$$\frac{L_xL_y}{2}\left\{-\left(\frac{1}{R_x\cos^2\alpha/2}+\frac{\nu}{R_y\cos\alpha/2\cos\beta/2}\right)\frac{1}{L_x}\left(u_{i+1j}-u_{i-1j}\right)\right.$$

$$-\left(\frac{1}{R_y\cos^2\beta/2}+\frac{\nu}{R_x\cos\alpha/2\cos\beta/2}\right)\frac{1}{L_y}\left(v_{ij+1}-v_{ij-1}\right)+\left(\frac{1}{R_x^2\cos^2\alpha/2}\right.$$

$$\left.+\frac{1}{R_y^2\cos^2\beta/2}+\frac{\nu}{R_xR_y\cos\alpha/2\cos\beta/2}\right)w_{ij}-\frac{1-\nu}{L_xL_y}\frac{d}{L_y}\left(u_{ij+1}-u_{ij-1}\right)$$

$$-\frac{1-\nu}{L_xL_y}\frac{d}{L_x}\left(v_{i+1j}-v_{i-1j}\right)+\frac{1-\nu}{L_xL_y}\frac{2d^2}{L_xL_y}w_{ij}+\frac{t^2}{4R_x\cos^2\alpha/2}\frac{1}{L_x^3}\left(u_{i+3j}\right.$$

$$-3u_{i+1j} + 3u_{i-1j} - u_{i-3j}) + \frac{t^2}{4R_y \cos^2 \beta/2} \frac{1}{L_y^3} (v_{ij+3} - 3v_{ij+1} + 3v_{ij-1} - v_{ij-3})$$

$$+ \frac{t^2}{4R_x \cos \alpha/2} \left[\frac{\nu}{\cos \beta/2} + \frac{1-\nu}{2} \left(\frac{1}{\cos \alpha/2} + \frac{1}{\cos \beta/2}\right)\right] \frac{1}{L_x L_y^2} (u_{i+1j+2} - 2u_{i+1j}$$

$$+ u_{i+1j-2} - u_{i-1j+2} + 2u_{i-1j} - u_{i-1j-2}) + \frac{t^2}{4R_y \cos \beta/2} \left[\frac{\nu}{\cos \alpha/2}\right.$$

$$\left. + \frac{1-\nu}{2} \left(\frac{1}{\cos \alpha/2} + \frac{1}{\cos \beta/2}\right)\right] \frac{1}{L_x^2 L_y} (v_{i+2j+1} - 2v_{ij+1} + v_{i-2j+1} - v_{i+2j-1}$$

$$+ 2v_{ij-1} - v_{i-2j-1}) + \frac{t^2}{4 \cos^2 \alpha/2} \frac{1}{L_x^4} (w_{i+4j} - 4w_{i+2j} + 6w_{ij} - 4w_{i-2j}$$

$$+ w_{i-4j}) + \frac{t^2}{4 \cos^2 \beta/2} \frac{1}{L_y^4} (w_{ij+4} - 4w_{ij+2} + 6w_{ij} - 4w_{ij-2} + w_{ij-4})$$

$$+ \frac{t^2}{4} \left[\frac{2\nu}{\cos \alpha/2 \cos \beta/2} + \frac{1-\nu}{2} \left(\frac{1}{\cos \alpha/2} + \frac{}{\cos \beta/2}\right)^2\right] \frac{1}{L_x^2 L_y^2} (w_{i+2j+2} - 2w_{i+2j}$$

$$\left. + w_{i+2j-2} - 2w_{ij+2} + 4w_{ij} - 2w_{ij-2} + w_{i-2j+2} - 2w_{i-2j} + w_{i-2j-2})\right\}$$

$$- \frac{1-\nu^2}{Eh} \bar{Z} = 0 \qquad \text{(A-3)}$$

APPENDIX B

A GENERAL DISCUSSION OF THE COMPUTER PROGRAM

To make greater use of the storage capacity of the computer, the entire process of generating and solving the set of equilibrium equations is accomplished by three sequential programs.

In the first program the shell dimensions and properties are read to the computer. The equilibrium equations are then generated and stored on an auxiliary tape. The strain-displacement relations corresponding to a given set of boundary conditions are made available to the computer by means of three FUNCTIONS. The loading is computed by a SUBROUTINE. By changing the FUNCTIONS or the SUBROUTINE, the same program can be used for a variety of boundary conditions or different loading combinations. In order to store the equilibrium equations in the least numbers of locations, the grid points are numbered in a one-dimensional triangular pattern. Furthermore, only the coefficients of displacements between the first and the last non-zero columns in each equation are stored. When a displacement component is zero, the point is not given a virtual displacement, thus no equation is generated at that point.

In the second program, the equilibrium equations are read back from the auxiliary tape to the computer one at a time. Gauss elimination method is used to reduce the matrix of coefficients to an upper triangular matrix. The solution is obtained by back substitution, starting with the last equation in the matrix and the results are then stored on an auxiliary tape. The maximum number of equations that can be solved depends on the storage capacity

of the computer and the maximum band width (the band width is defined as the number of terms between the first and the last non-zero columns in an equation) of the equations.

In the third program the results are read back from the auxiliary tape to the computer. The strains, the forces, and the moments are computed and the desired values are printed out.

A general flow diagram of the computer program is shown in Fig. B-1.

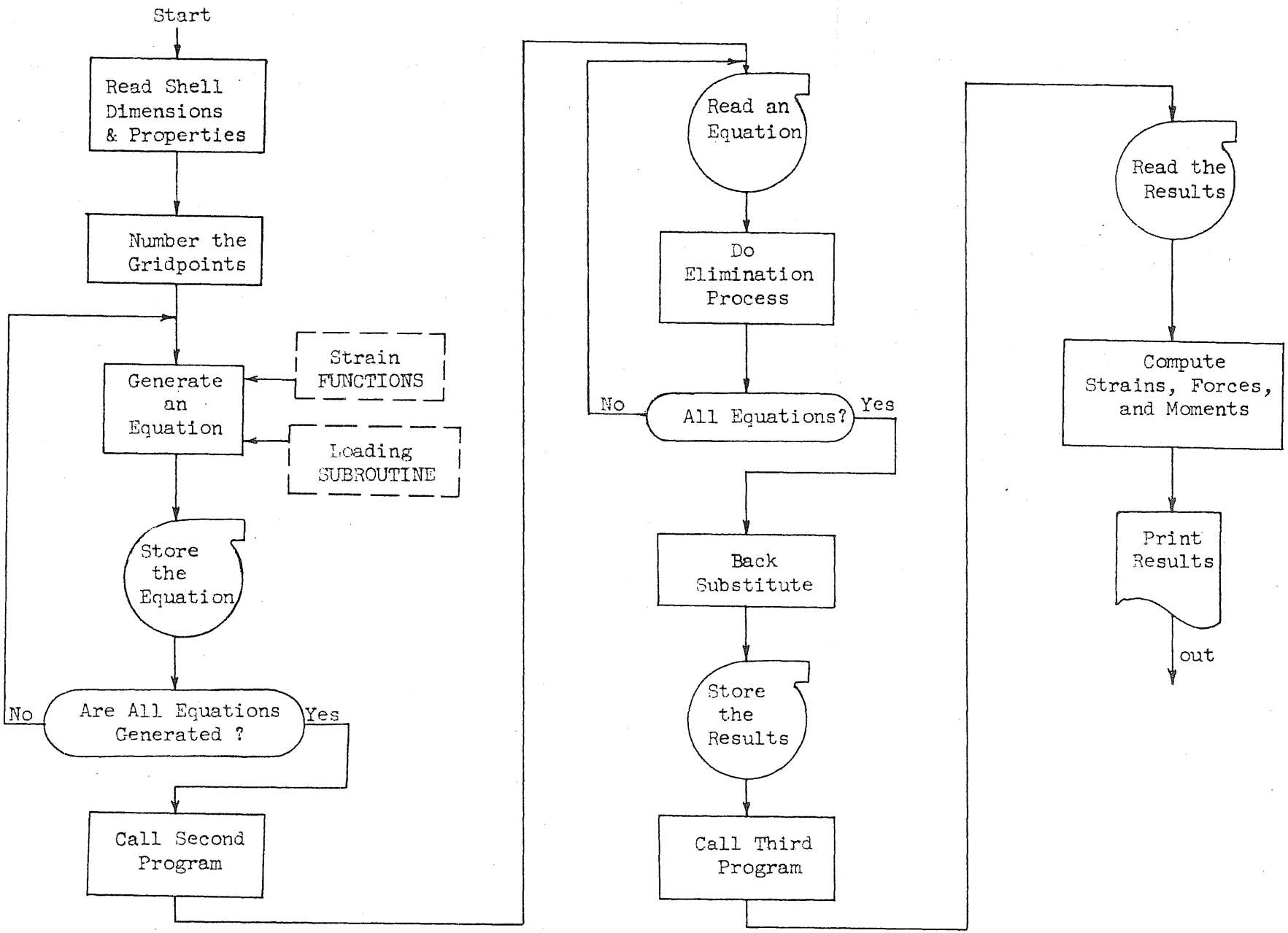

FIG. B-1 GENERAL FLOW DIAGRAM OF THE COMPUTER PROGRAM